Computational and Structural Biotechnology Journal 19 (2021) 4517–4537

COMPUTATIONAL AND STRUCTURAL BIOTECHNOLOGY JOURNAL

journal homepage: www.elsevier.com/locate/csbj

Neuroprotective derivatives of tacrine that target NMDA receptor and acetyl cholinesterase – Design, synthesis and biological evaluation

Chandran Remya [a], K.V. Dileep [b,c,1], Eeda Koti Reddy [d,1], Kumar Mantosh [e,1,2], Kesavan Lakshmi [e,2], Reena Sarah Jacob [e,3], Ayyiliyath M. Sajith [f], E. Jayadevi Variyar [a], Shaik Anwar [d], Kam Y.J. Zhang [b], C. Sadasivan [a], R.V. Omkumar [e,*]

[a] Department of Biotechnology and Microbiology, Kannur University, Dr. Janaki Ammal Campus, Thalassery, Kerala 670661, India
[b] Laboratory for Structural Bioinformatics, Center for Biosystems Dynamics Research, RIKEN, 1-7-22 Suehiro, Tsurumi, Yokohama, Kanagawa 230-0045, Japan
[c] Laboratory for Computational and Structural Biology, Jubilee Center for Medical Research, Jubilee Mission Medical College and Research Institute, Thrissur, Kerala 680005, India
[d] Division of Chemistry, Department of Sciences and Humanities, Vignan's Foundation for Sciences, Technology and Research -VFSTR (Deemed to be University), Vadlamudi, Guntur, Andhra Pradesh 522 213, India
[e] Molecular Neurobiology Division, Rajiv Gandhi Centre for Biotechnology, Thycaud PO, Thiruvananthapuram, Kerala 695014, India
[f] Post Graduate and Research Department of Chemistry, Kasaragod Govt. College, Kannur University, Kasaragod, India

ARTICLE INFO

Article history:
Received 29 March 2021
Received in revised form 28 July 2021
Accepted 29 July 2021
Available online 3 August 2021

Keywords:
Alzheimer's disease
MTDLs
Structure-based drug design
Polypharmacology
Tacrine
Acetylcholinesterase
NMDA receptor
Neuroprotection

ABSTRACT

The complex and multifactorial nature of neuropsychiatric diseases demands multi-target drugs that can intervene with various sub-pathologies underlying disease progression. Targeting the impairments in cholinergic and glutamatergic neurotransmissions with small molecules has been suggested as one of the potential disease-modifying approaches for Alzheimer's disease (AD). Tacrine, a potent inhibitor of acetylcholinesterase (AChE) is the first FDA approved drug for the treatment of AD. Tacrine is also a low affinity antagonist of N-methyl-D-aspartate receptor (NMDAR). However, tacrine was withdrawn from its clinical use later due to its hepatotoxicity. With an aim to develop novel high affinity multi-target directed ligands (MTDLs) against AChE and NMDAR, with reduced hepatotoxicity, we performed *in silico* structure-based modifications on tacrine, chemical synthesis of the derivatives and *in vitro* validation of their activities. Nineteen such derivatives showed inhibition with IC_{50} values in the range of 18.53 ± 2.09 – 184.09 ± 19.23 nM against AChE and 0.27 ± 0.05 – 38.84 ± 9.64 μM against NMDAR. Some of the selected compounds also protected rat primary cortical neurons from glutamate induced excitotoxicity. Two of the tacrine derived MTDLs, 201 and 208 exhibited *in vivo* efficacy in rats by protecting against behavioral impairment induced by administration of the excitotoxic agent, monosodium glutamate. Additionally, several of these synthesized compounds also exhibited promising inhibitory activitiy against butyrylcholinesterase. MTDL-201 was also devoid of hepatotoxicity *in vivo*. Given the therapeutic potential of MTDLs in disease-modifying therapy, our studies revealed several promising MTDLs among which 201 appears to be a potential candidate for immediate preclinical evaluations.

Abbreviations: AD, Alzheimer's disease; AChE, acetylcholinesterase; NMDAR, N-methyl-D-aspartate receptor; MTDLs, multi-target directed ligands; AChEIs, acetylcholinesterase inhibitors; TBI, traumatic brain injury; MWM, Morris water maze; RMSD, root mean square deviation; MD, Molecular dynamics; LBD, Ligand binding domain; TMD, transmembrane domain; ChE, Cholinesterases; Ca^{2+}, calcium; MAP2, microtubule associated protein 2; G6PD, glucose-6-phosphate dehydrogenase; IP, intraperitoneal; BBB, blood brain barrier; SVM, support vector machine; LiCABEDS, Ligand Classifier of Adaptively Boosting Ensemble Decision Stumps; SAR, structure-activity relationships; NMA, normal mode analysis; ENM, elastic network modeling; h-NMDAR, human NMDAR; hAChE, human AChE; ADME, absorption, distribution, metabolism and excretion; OPLS, Optimized potential for liquid simulations; ppm, parts per million; LC-MS, Liquid chromatography-mass spectrometry; DTNB, 5,5-dithiobis-(2-nitrobenzoic acid); AChT, acetylthiocholine; DMEM, Dulbecco's modified Eagle's medium; HBSS, Hank's balanced salt solution; PFA, paraformaldehyde; ER, endoplasmic reticulum; FRET, fluorescence resonance energy transfer; PBS, phosphate-buffered saline; NBM, neurobasal medium; SD, standard deviation.

* Corresponding author.
E-mail address: omkumar@rgcb.res.in (R.V. Omkumar).

[1] K.V.D, E.K.R and M.K contributed equally.
[2] Research scholar, University of Kerala, India.
[3] Research scholar, Manipal Academy of Higher Education, Manipal 576 104, India.

https://doi.org/10.1016/j.csbj.2021.07.041

1. Introduction

Alterations in the levels of various neurotransmitters and functioning of neuronal networks in the brain lead to neuropsychiatric disorders. Alzheimer's disease (AD) is a condition in which various factors such as impairment in cholinergic and glutamatergic signaling, toxicity due to accumulation of Aβ peptides and hyperphosphorylated tau proteins, neuroinflammation, metal dyshomeostasis, oxidative stress, mitochondrial dysfunction and genetic predisposition contribute to the pathological events leading to cognitive decline and neurodegeneration [1–3]. A detailed review on AD pathophysiology, treatment options, risk factors and epidemiology has been published recently [4]. Correlation between cholinergic dysfunction and AD progression prompted the identification of several potential disease-modifying agents such as acetylcholinesterase inhibitors (AChEIs) and acetylcholine receptor agonists for improving cholinergic functions [5–11]. AChEIs such as donepezil [12], galantamine [13] and rivastigmine [14] are currently being used for the treatment of moderate to severe AD. Though these drugs are beneficial in improving cognitive and behavioral symptoms, they do not prevent the process of neurodegeneration completely.

Neuronal loss that occurs in the brain is an underlying factor for AD [15,16] and for other neurodegenerative diseases [17]. Abnormal release of glutamate and/or deficiency of glutamate uptake mechanisms result in the accumulation of extracellular glutamate leading to neuronal apoptosis, a process termed as excitotoxicity that happens by the overactivation of the N-methyl-D-aspartate type glutamate receptor (NMDAR) [18–20]. The role of NMDAR in AD has recently been reviewed by Liu et al. [21]. NMDAR antagonists are suggested to act as therapeutic agents for this condition [20,22]. Excitotoxicity triggered by Aβ peptides and tau proteins have been prevented by NMDAR antagonists like memantine and ifenprodil [23–25]. Memantine is one of the FDA approved drugs used for the treatment of moderate to severe AD [26]. According to the current clinical data, combination therapy with memantine and AChEIs produces benefits in all stages of AD than the monotherapies [27–32].

In conditions like oxygen-glucose deprivation in brain slices [33] and in NMDA-induced excitotoxicity in cultured neurons [34], the role of NMDAR as a potential target for neuroprotection has already been demonstrated. Variations in NMDAR activity are associated with ischemic conditions [35], stroke [36], traumatic brain injury (TBI) [37], glioma [38] and neuropsychiatric diseases [39–40], suggesting the therapeutic potential of NMDAR modulators in these conditions. The involvement of NMDARs in pain circuitries makes it a potential target for analgesic drugs [41]. However, many NMDAR antagonists currently in clinical use either have insufficient efficacy or have undesirable side effects. Hence, new and better antagonists are necessary for treating neurological diseases.

Tacrine, a potent inhibitor of AChE [42] is the first FDA approved drug for the treatment of AD but had hepatotoxicity that led to its withdrawal from clinical use [43]. Interestingly, tacrine was also reported as a weak antagonist of NMDAR [44]. Hence, tacrine is unlikely to cause NMDAR inhibition at its therapeutic dose required to achieve AChE inhibition. This also makes tacrine an unsuitable candidate for the treatment of other neurological conditions such as stroke and traumatic brain injury where NMDAR antagonists would be useful. Chemical modification of tacrine may help to improve its inhibitory potency towards NMDAR. This may also permit reducing the dosage so that hepatotoxicity could be brought within safety limits. Despite its hepatotoxicity, tacrine structure has been successfully used in medicinal chemistry for designing hybrids and multi-target directed ligands (MTDLs) [45–55].

Due to the complex etiology and multi-faceted nature of AD, use of MTDLs has been suggested as a promising treatment strategy. Compared to the mono and combination therapies, MTDLs have advantages [56] such as lower probabilities of drug-drug interactions, reduced off-target interactions, wider therapeutic window and improved safety profiles [57,58]. Though several MTDLs were shown to be effective *in vitro*, success rate in the preclinical/clinical stages have been highly limited. By combining molecules such as donepezil, galantamine, rivastigmine and tacrine with each other and with other chemical entities, several MTDLs have been suggested [59]. Several MTDLs have been suggested for preclinical studies for use in AD [60,61]. Two MTDLs that are in the clinical trial have failed recently. This has necessitated the need for more research on MTDLs and other disease modifying agents [62].

In the current study, with an aim to propose novel, high affinity and less hepatotoxic tacrine derived MTDLs that can modulate the dysfunctions in cholinergic and glutamatergic systems, we systematically designed, synthesized and evaluated a series of MTDLs against the two promising drug targets, AChE and NMDAR. Similar studies on tacrine derivatives that are dually active against AChE and NMDAR have recently been published [63–66]. Effects of MTDLs on rat primary cortical neurons under excitotoxic conditions were also studied. Neuroprotective effects of selected MTDLs were also assessed using Morris water maze test (MWM) for behavioral study of rats.

2. Results

2.1. Molecular modeling studies

2.1.1. Coarse-grained modeling provided h-NMDARs with multiple receptor conformations

High-resolution crystal structures of quasi-independent domains of NMDAR with different allosteric inhibitors have been reported [67,68]. However, structures representing the open and closed conformations of the channels were reported at moderate resolutions and hence could not be used for molecular modeling studies due to missing residues and side chains [69,70]. Reports from literature suggested that tacrine binds in the channel of NMDAR [71–76]. To decrypt the mode of binding of tacrine in the channel pore of NMDAR, we assumed that the structural dynamics of NMDAR have to be addressed. The GluN1/GluN2B subtype of NMDAR of *Xenopus laevis* possessed high sequence similarity (≥90%) to human-GluN1/GluN2B subtype of NMDAR. Hence, human NMDAR (h-NMDAR) was modelled by choosing the crystal structure of GluN1/GluN2B heteromer of *Xenopus laevis* in complex with MK-801 as the template. The missing regions in the template structure, such as loops were modeled and energy minimized. The lowest energy conformation was taken as the model for further studies. As expected the modeled structure showed high similarity to the template structure.

Since all atom molecular dynamics (MD) simulation was computationally very expensive, coarse-grained modeling technique was used to probe the dynamics of h-NMDAR. The observed structural dynamics in the coarse-grained modeling were assumed to be representing various biological functional states such as open and closed conformations of the channel. The normal mode analysis (NMA) and elastic network modeling (ENM) simulations retrieved 339 output structures, which were gathered and checked for the global root mean square deviation (RMSD) by superimposing them

with the modeled h-NMDAR. The superimposition studies revealed that RMSD varies from ~0.1 to 4 Å. Based on RMSD, the structures were classified into four clusters. Cluster-1 contains structures with RMSD 0.1–1 Å, cluster-2 with RMSD 1–2 Å, cluster-3 with RMSD 2–3 Å and cluster-4 with RMSD 3–4 Å (Fig. 1A). Since the template structure is in the open conformation, all the structures in cluster-1 were assumed to be representing an open conformation. Candidate structures were selected from each cluster and were used for docking studies.

The NMA and ENM simulations predicted two key motions featuring shearing/twisting for the ligand binding domains (LBDs) which are in concert with the transmembrane domains (TMD) (Fig. 1B). It was observed that D1 and D2 lobes of GluN2B move in opposite directions when compared to the motion of D1 and D2 lobes of GluN1, triggering an inward movement for the TMD. Our results are similar to the previously reported structural dynamics of NMDAR [77]. Since the modeled h-NMDAR was in open conformation, it is assumed that, the observed structural dynamics in the coarse-grained modeling might be representing partially or fully closed conformations. In our coarse-grained modeling, it was also observed that the structural changes were transmitting from LBD to TMD through linkers that connect the LBD and three transmembrane helices M1, M3, and M4 at TMD. The surface area of the channel in the candidate structures (denoted as NMDAR-1 to NMDAR-4) were found to be 1269, 832, 801 and 543 $Å^2$ respectively. Hence, it is assumed that the conversion from NMDAR-1 to NMDAR-4 might be representing the transformation from open (NMDAR-1) to partially closed (NMDAR-2/3) and to fully closed conformations (NMDAR-4).

2.1.2. Binding studies of tacrine towards NMDAR revealed that it binds in the MK-801 binding pocket

Further to understand the binding mode of tacrine, we performed ensemble docking against these four candidate structures. The binding energies of tacrine towards NMDAR-1 to NMDAR-4 are -68, -57, -51 and -38 kcal/mol and these binding energies are directly proportional to the size of the binding site. We selected the best scoring pose of tacrine and further analyzed the atomic interactions. In the most energetically favored binding mode of tacrine, it was observed that tacrine resides within the same pocket where MK-801 binds. Tacrine was oriented in the channel vestibule in such a way that it can form a hydrogen bond with the backbone atom of L643 of GluN2B (Fig. 1C). Other residues in the M3 helices of GluN1 and GluN2B chains were also contributing to the stability of binding.

2.1.3. The conformation of Y337 act as a key determinant in case of tacrine binding to AChE

Utilizing the ensemble docking approach, the binding energies of tacrine towards the selected AChE structures were determined. Tacrine was unable to bind to the apo (AChE-1) and donepezil bound (AChE-3) structures of AChE, due to steric clashes with Y337. Since the side chain orientation of Y337 was favorable in huperzine bound (AChE-2) and 9-aminoacridine bound (AChE-4) structures, tacrine was able to bind to the active site gorge. Binding energies of tacrine towards AChE-2 and AChE-4 were −42 and −79 kcal/mol respectively. It has been reported that the side chain of Y337 acts as a swinging gate and plays an important role in recognizing different ligands [78]. In the lowest energy pose, tetrahydroacridine moiety of tacrine is sandwiched between W86 and Y337 and thus favored face to face π-π stacking interactions. Similarly, W439 is involved in the edge to face stacking interactions with tacrine. Additionally, a hydrogen bond was observed between backbone O atom of H447 and N atom of tacrine (Fig. 1D). Binding energies of tacrine towards NMDAR-1 to 4 and AChE-1 to 4 are denoted in Fig. 1E.

2.1.4. Structure based design provided several tacrine derived MTDLs

Our critical investigation of the binding modes of tacrine on NMDAR and AChE revealed additional room for modifications. We were interested in the four potential pharmacophoric regions in tacrine, represented as R1 to R4 for the designing of potential MTDLs, where R1, R2 are located in the cyclohexane ring and R3, R4 are located in the aromatic ring of tacrine (Fig. 1F). In case of NMDAR, we found that three hydrogen bond donors (backbone nitrogen atoms of V640, I641 and A644 of GluN2B) and two hydrogen bond acceptors (backbone oxygen atoms of A639 and V640 of GluN2B) are located within 6 Å distance from the R1 position. Hence, we assumed that the substitution of hydrogen bond donors or acceptors at R1 position may favor hydrogen bonding and thus improve the binding affinity towards NMDAR. We then investigated whether these substitutions would also favor the binding towards AChE. In our previous studies, we demonstrated that substitution at R1 position significantly improved the binding affinities of novel tacrine derivatives [55]. Although, the phenylethylacetamide and phenylpropylacetamide in compounds 6b, 6c, 6e, 6f, 6h, 6i and 6j maintained AChE inhibitory activities [55], we did not include such bulky substitutions in the current study due to possible steric clashes with residues in the M3 helices of both GluN2B and GluN1.

We then investigated the possibilities of R2 substitutions. In case of NMDAR, we found only two hydrogen bond donors (hydroxyl group at the side chain of T648 and backbone N atom of A645 of GluN1) at a distance of 5 Å from the R2 position. In case of AChE, we found that the R2 position is not favorable for substitution due to possible steric clashes with the side chain of E202 and backbone N atoms of G120 and G121. All these residues were located within 3.5 Å from R2 position. Hence, we omitted R2 position from further substitutions in the current study.

Our next step was to investigate the possibilities of R3 and R4 substitutions. In our previous studies, we successfully demonstrated that substitutions of bromine and aromatic moieties such as methylpyrazole and pyrimidine at R4 position maintained the AChE inhibitory activity [55]. In case of NMDAR, an aromatic cage constituted by the following residues, F548, F554, W563, Y647 (from GluN1) and F637 (from GluN2B) is situated at a distance of 10 Å from both R3 and R4. At the same time, in AChE, any bulky aromatic substitution at R3 position may cause steric clashes with Y341. Based on this observation we decided to eliminate R3 position for further modifications in the current study. Moreover, we also found that any bulky aromatic substitutions at R4 position may introduce stacking interactions with W439 and Y449 of AChE. Based on all these observations we designed 75 ligands and grouped them into three different groups where group-1 consists of ligands that are having substitutions only at R1, group-2 consists of ligands having substitution only at R4 and group-3 consists of ligands with substitutions at both R1 and R4 (Table S1). We then performed ensemble docking studies for all the ligands against both NMDAR and AChE and binding energies were determined. We found the binding energies vary from −10 to −90 kcal/mol towards NMDAR and −10 to −120 kcal/mol towards AChE (Fig. 1G).

2.1.5. In silico binding affinity guided the selection of tacrine derived MTDLs for synthesis

Though we designed 75 compounds based on the pharmacophoric features derived from tacrine binding, we synthesized only 19 tacrine derived MTDLs for further evaluations. The compounds are named according to our patent application (IPO-201841015699). Corresponding numbers of these compounds in the *in silico* designs are shown in Table S1. ADME properties and binding affinities predicted *in silico* in the current study encouraged us to choose compounds 16 and 17 of group-1, 201, 203–

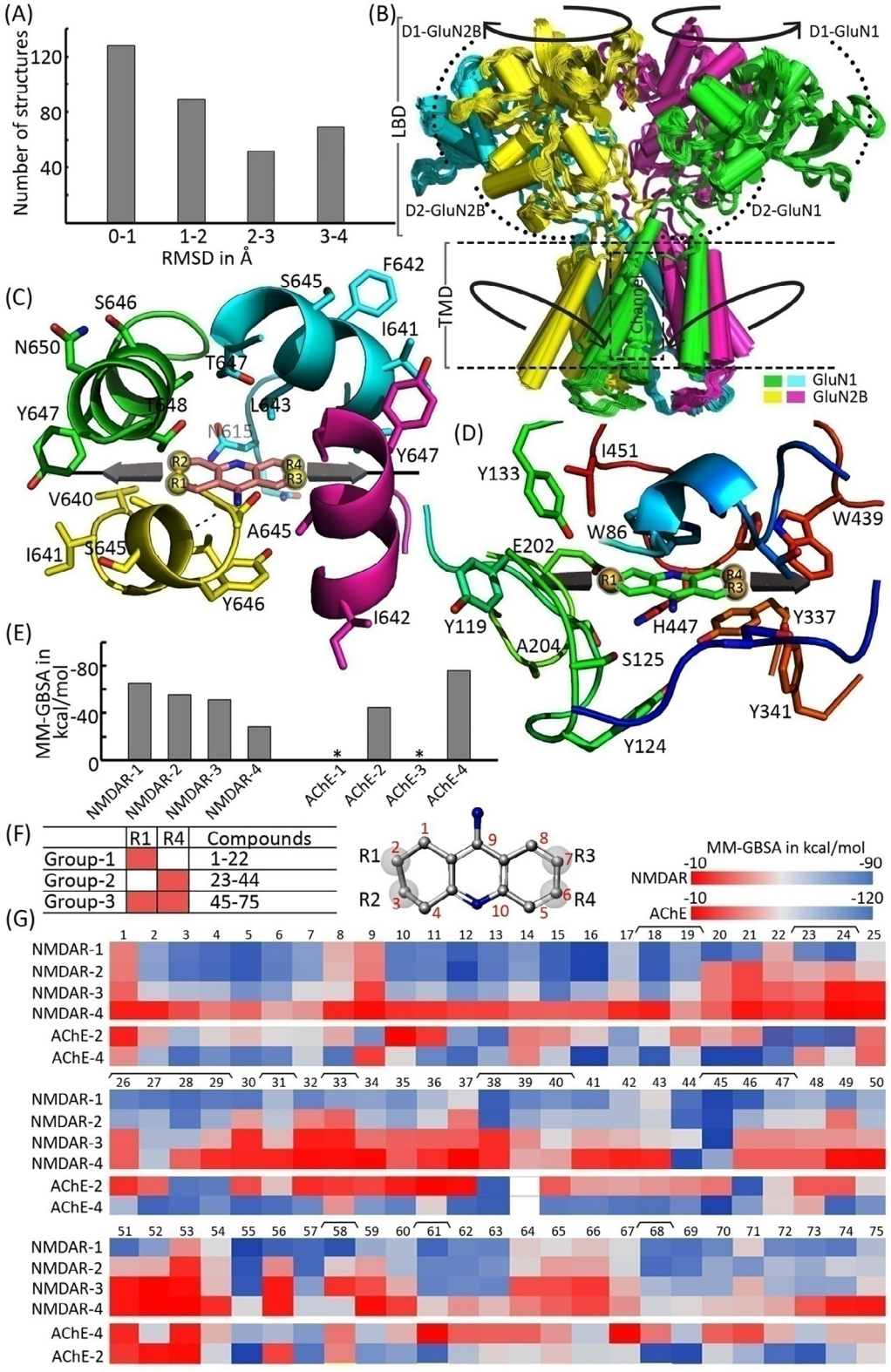

Fig. 1. Modeling of h-NMDAR and docking of tacrine derived MTDLs against NMDAR and AChE. (A) RMSD based clustering of output structures obtained from the coarse-grained modeling of NMDAR. (B) Structure of modeled heteromeric h-NMDAR composed of two subunits each of GluN1 (shown in green and cyan color) and GluN2B (shown in yellow and magenta color). Two key motions featuring shearing/twisting for the ligand binding domain (LBD) (indicated by arrows pointing outwards) and transmembrane domain (TMD) (indicated by arrows pointing inwards) are also shown. (C) Binding mode of tacrine (salmon stick) in the channel vestibule of the modeled h-NMDAR. The possible sites available for modifications on tacrine are also denoted as R1 to R4. (D) Binding mode of tacrine (green stick) in the active site of human AChE. (E) Binding energies (MM-GBSA in kcal/mol) obtained for tacrine from the ensemble docking, where * indicates absence of a biologically significant docked pose. Candidate structures of h-NMDAR and human AChE (hAChE) used for ensemble docking are represented as NMDAR-1 to NMDAR-4 and AChE-1 to AChE-4 respectively. (F) Three-dimensional structure of tacrine marked with available sites for modifications (R1-R4) and numbers assigned to MTDLs that belong to different groups based on the substitutions are also shown. (G) Heatmap of the binding energies (MM-GBSA in kcal/mol) obtained for designed MTDLs after ensemble docking. Ligands that are synthesized in the current study (MTDLs-18, 19, 23, 24, 26–29, 31, 33, 38–40, 45–47, 58, 61 and 68) are marked. (For interpretation of the references to color in this figure legend, the reader is referred to the web version of this article.)

206, 208–212 and 214 of group-2 and 5, 8, 10, 13, 14 and 107 of group-3 for synthesis and further evaluations. No structural alert was found when they were screened for Pan assay interference of compounds (PAINS) using SwissADME tool. The physicochemical properties predicted using the QikProp module for the selected MTDLs are listed in Table S2. The predictions indicate that all compounds have general drug like properties except 206 and 211. The LogP values of these two compounds were slightly higher, but it has already been reported that CNS active ligands can have higher LogP (more lipophilic) values compared to general therapeutics [79,80] and hence they were included in further studies.

2.2. Synthesis of selected tacrine derived MTDLs

All the selected MTDLs were synthesized by the reaction procedures described in Schemes 1 and 2 and the final products were characterized by ^{1}H NMR, ^{13}C NMR and LCMS. The 6-bromo tacrine (3) was synthesized by condensation of 4-bromo-2-amino benzonitrile (1) and cyclohexanone (2) in presence of borane trifluoro etherate ($BF_3.Et_2O$) under reflux for 4 h. The palladium-mediated Suzuki-Miyaura cross coupling reaction of compound 3 with corresponding boronic acids or boronic esters (4a-4m described in Experimental section) resulted in the title compounds 201 and 203–214. Similar procedure was adopted to get the compounds 05, 16, 10 and 107. Compounds 05 and 10 were further treated with aqueous methyl amine to synthesize compounds 13 and 14 respectively. The compounds 17 and 08 were synthesized from 16 and 05 respectively by reacting with hydrazine hydride.

2.3. In vitro studies

2.3.1. Tacrine derived MTDLs inhibit cholinesterases (ChE)

Ellman's method based ChE assay revealed varying degrees of inhibitory activities for MTDLs on ChEs. Our IC_{50} evaluation of tacrine against BChE from equine serum (IC_{50} = 14.26 ± 1.07 nM) and AChE from electric eel (IC_{50} = 94.69 ± 4.88 nM) confirmed the selectivity of tacrine towards BChE over AChE as reported in literature [81]. The IC_{50} values of all MTDLs against AChE were in the nM range and towards BChE were in the μM range (Table 1). Hence, we concluded that these MTDLs except 208 were more selective towards AChE than BChE.

Our detailed analysis of the IC_{50} values revealed that 11 (Compound numbers-13, 16, 17, 201, 203, 205, 208, 209, 211, 212 and 214) out of 19 compounds exhibited higher inhibition towards AChE from electric eel than tacrine. Among these compounds, compound 203, having a pyrimidine ring connected to the R4 position has an excellent anti AChE activity (IC_{50} = 18.53 ± 2.09 nM). Substitutions of methyl pyrazole (compound 201, IC_{50} = 40.89 ± 4.82 nM) and fluoro benzene (compound 209, IC_{50} = 76 ± 3.79 nM) at R4 position of tacrine were found to have more inhibitory potency compared to compounds with substitutions at R1 position (compounds 10: IC_{50} = 107.17 ± 8.68 nM, 14: IC_{50} = 131.92 ± 7.72 nM and 107: IC_{50} = 135.11 ± 10.25 nM). Simple halogen substitutions at R4 position along with substitutions at R1 position (compounds 5: IC_{50} = 100.4 ± 7.2 nM and compound 8: IC_{50} = 137.7 ± 16.1 nM) exhibited less inhibitory activity when compared to substitutions at R1 alone (compounds 16: IC_{50} = 42.2 ± 2.7 nM and 17: IC_{50} = 1 9.27 ± 0.47 nM). The study also revealed that compounds with simple aromatic ring at R4 position (compounds 201, 203, 212 and 214) are preferred over those compounds with substituted aromatic rings (compounds 205, 206, 208, 209, 210 and 211).

2.3.2. Improved antagonistic potential of tacrine derived MTDLs towards NMDAR

The effect of MTDLs on NMDAR activity was evaluated using a cell-based assay system, in which the appearance of fluorescent punctate pattern occurred upon activation of NMDAR by its agonists in presence of calcium (Ca^{2+}) (Fig. 2B (i)) [82]. The punctate appearance was absent when NMDAR was treated with its agonists in the absence of Ca^{2+} (Fig. 2B (ii)), which clearly indicated that the assay system is dependent on Ca^{2+} influx through NMDARs. Activation of NMDAR in presence of the MTDLs resulted in the reduction of the number of cells with punctate pattern which is positively correlated to the inhibition of Ca^{2+} influx through NMDAR. Initially, two different concentrations (50 and 100 μM) of the compounds were tested for their effect on NMDAR activity.

All MTDLs except tacrine and compounds 5, 8, 13, 16 and 17 exhibited > 60% inhibition of NMDAR activity (Fig. 2A). Almost 100% inhibition was observed for the compounds 201, 204, 205, 206, 208, 209, 210 and 211 at 100 μM and for compounds 208, 209, 210 and 211 this happened at 50 μM itself. Further, their inhibitory potency at 20 μM was also tested in order to determine the concentration range for inhibition. From the initial screening studies, it was found that MTDLs belonging to group-2 having substitutions only at R4 position (i.e., compounds 201, 203, 204, 205, 206, 208, 209, 210, 211, 212 and 214) were effective in antagonizing NMDAR activity while the compounds belonging to group-1 where the substitution was only at R1 position (compounds 16 and 17) could not effectively block NMDAR activity. MTDLs that belong to group-3 with dual substitutions i.e., aromatic substitutions at R4 and substitutions at R1 positions (compounds-10, 14 and 107) inhibited NMDAR activity better when compared to simple halogen substitutions at R4 position (compounds 5, 8 and 13). Hence, we inferred that aromatic substitutions at R4 position alone might be sufficient to antagonize NMDAR activity, which is corroborated by IC_{50} determinations. It was clear from the measured IC_{50} values (Table 1) that the inhibitory potency of some MTDLs (208, IC_{50} = 0. 31 ± 0.09 μM and 210, IC_{50} = 0.27 ± 0.05 μM) were almost 600 fold higher when compared to the reported value for tacrine (IC_{50} = 1 93 ± 33 μM) [44]. About 4 fold increase in potency was observed for compound 209 (IC_{50} = 3.36 ± 0.86 μM) when compared to 107 (IC_{50} = 15.81 ± 3.44 μM) and the potency was further increased upto 10 fold by halogen substitution at ortho position of phenyl ring at R4 position of tacrine (compound 208). Representative images showing NMDAR activities in presence of agonists and in the presence of compounds 211 and 208 are shown in Fig. 2B (iii and iv).

2.3.3. MTDLs do not interfere with the interaction between GluN2B and α-CaMKII

In the NMDAR assay, activity is detected based on the formation of punctae as a result of Ca^{2+}-dependent protein–protein interaction between α-CaMKII and GluN2B subunit of NMDAR. Any agent which can block the interaction between these two proteins may reduce or completely inhibit the appearance of punctae. This reduction in punctae however, would not be due to the blocking of NMDAR channel activity. To test whether the compounds have any effect on the interaction of GluN2B and α-CaMKII, an experiment was carried out using HEK-293 cells stably expressing GFP-α-CaMKII and GluN2B sequence [82]. Formation of perinuclear punctae by treatment with ionomycin and Ca^{2+}, is indicative of interaction between α-CaMKII and GluN2B. No detectable reduction in punctae formation, in presence of the MTDLs, confirmed that the compounds do not have any effect on the interaction of GluN2B and α-CaMKII (Figs. S2 and S3).

2.4. MTDLs are less cytotoxic than tacrine on HepG2 cells

Since hepatotoxicity is one of the serious concerns with new tacrine derivatives, we checked the cytotoxic nature of all derivatives on the liver carcinoma cell line, HepG2 using 3-(4,5-dimethyl thiazol-2-yl)-2,5-diphenyltetrazolium bromide (MTT) assay.

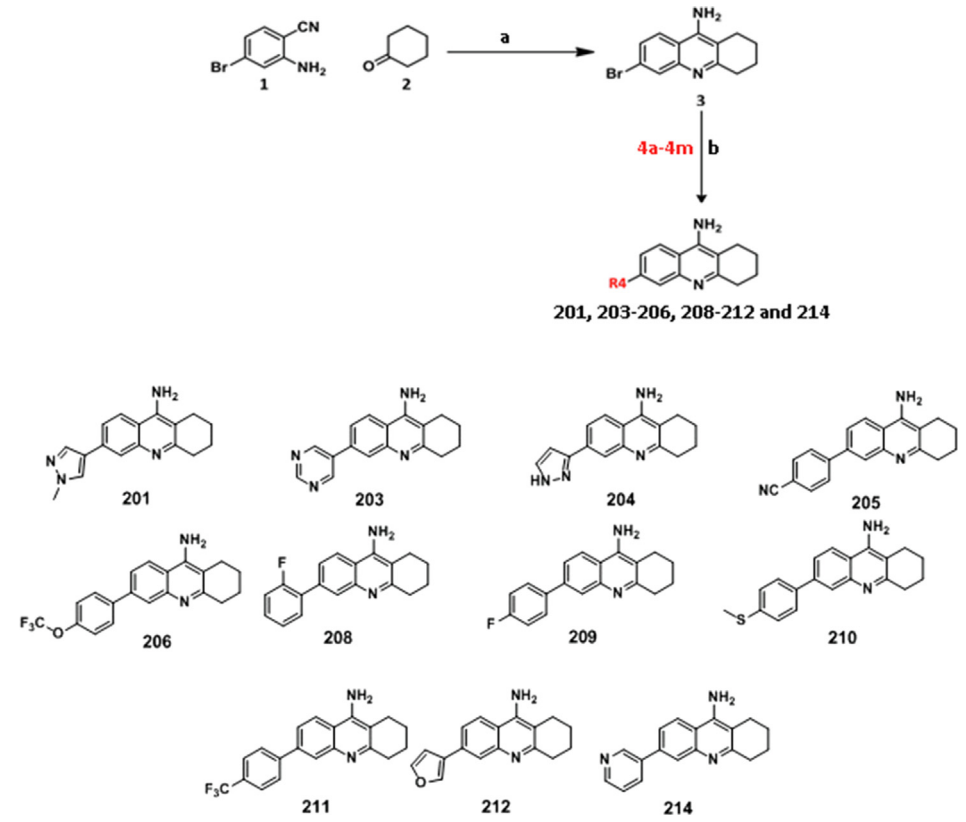

Scheme 1. Synthesis scheme for R4-substituted tacrine derivatives. **Reagents and conditions**: (a) $BF_3.Et_2O$, toluene, 110 °C, 4 h (b) compounds **4a**-**4m** (structure of these chemicals are given in Fig. S1), Na_2CO_3, $Pd(PPh_3)_4$, 1,4-dioxane and water (9:1), 110 °C, 2 h, sealed tube.

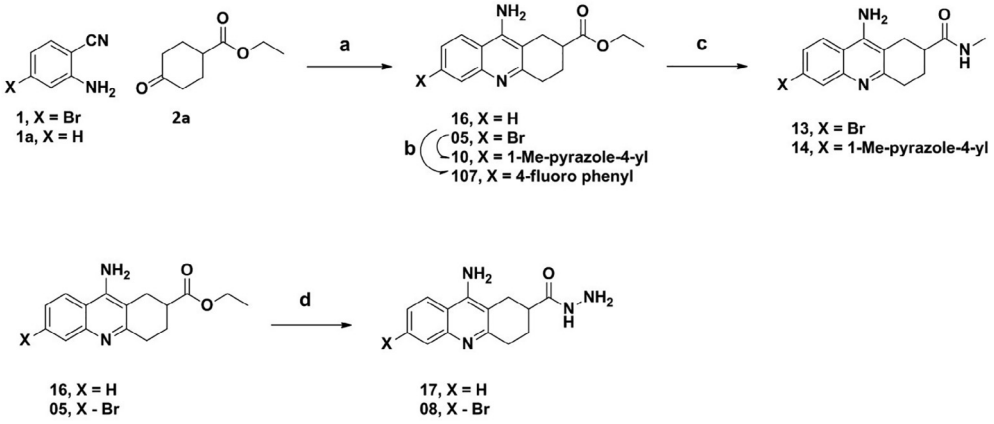

Scheme 2. Synthesis scheme for R1 and R4-substituted tacrine derivatives. **Reagents and conditions:** (a) $BF_3.Et_2O$, toluene, 110 °C, 4 h (b) compound **4a** for **10** and **4h** for **107**, Na_2CO_3, $Pd(PPh_3)_4$, 1,4-dioxane and water (9:1), 110 °C, 2 h, sealed tube; (c) aq.$MeNH_2$, 60 °C, 4 h; (d) $NH_2NH_2{\cdot}H_2O$, 60 °C, 2 h.

HepG2 cell line is one of the widely used *in vitro* models to study hepatotoxicity of chemicals [83–85]. As seen in Fig. 2C, tacrine was safe only up to 50 μM and the cell viability decreased from 100 μM onwards. At 300 μM, almost 50% reduction in cell viability was observed. Almost all tacrine derived MTDLs tested were found to be less toxic than tacrine (approximately > 80% cell viability at 300 μM). Compounds such as 14, 201, 204, 209, 212 and 214 were non-toxic even at a concentration of 300 μM.

2.5. Neuroprotective properties of tacrine derivatives

2.5.1. Establishment of glutamate toxicity model in rat primary cortical neurons

The neuroprotective properties of selected MTDLs were evaluated against glutamate induced excitotoxicity in primary cortical neurons prepared from the brain of embryonic rats. Cortical neurons were maintained in culture and excitotoxicity experiments were performed on the 9th day of culture (DIV9). Previous studies demonstrated that neurons at DIV9 are appropriate to study glutamate toxicity as the cells are mature enough in terms of NMDA receptor expression and glutamate sensitivity [86–90]. An *in vitro* excitotoxicity model was established by treating cortical neurons with 100 μM glutamate for 1 h followed by analysis at 24 h post

Table 1
Results of AChE, BChE and NMDAR inhibition studies of the tacrine derived MTDLs n.d indicates not determined.

		IC_{50} values (mean ± SD)		
Sl No	Compound numbers	AChE (nM)	BChE (μM)	NMDAR (μM)
1	5	100.4 ± 7.2	7.38 ± 0.21	n.d
2	8	137.7 ± 16.1	20.39 ± 2.11	n.d
3	10	107.17 ± 8.7	4.39 ± 0.28	31.12 ± 4.8
4	13	28.59 ± 3.59	47.29 ± 5.98	n.d
5	14	131.92 ± 7.7	16.39 ± 0.54	33.86 ± 8.41
6	16	42.2 ± 2.7	3.82 ± 0.25	n.d
7	17	19.27 ± 0.47	2.99 ± 0.40	n.d
8	107	135.11 ± 10.3	1.35 ± 0.09	15.81 ± 3.44
9	201	40.89 ± 4.82	0.85 ± 0.01	15.17 ± 6.14
10	203	18.53 ± 2.09	1.50 ± 0.20	28.1 ± 5.1
11	204	136.70 ± 7.35	0.96 ± 0.07	14.59 ± 4.32
12	205	84.17 ± 1.80	0.70 ± 0.08	2.84 ± 0.46
13	206	184.09 ± 19.23	1.21 ± 0.16	9.19 ± 2.68
14	208	75.07 ± 9.46	0.13 ± 0.02	0.31 ± 0.09
15	209	76.00 ± 3.79	1.03 ± 0.17	3.36 ± 0.86
16	210	149.27 ± 16.82	0.94 ± 0.12	0.27 ± 0.05
17	211	74.58 ± 8.29	3.97 ± 0.71	0.49 ± 0.14
18	212	53.59 ± 4.39	0.99 ± 0.05	16.43 ± 2.76
19	214	49.43 ± 2.37	0.82 ± 0.09	38.84 ± 9.64

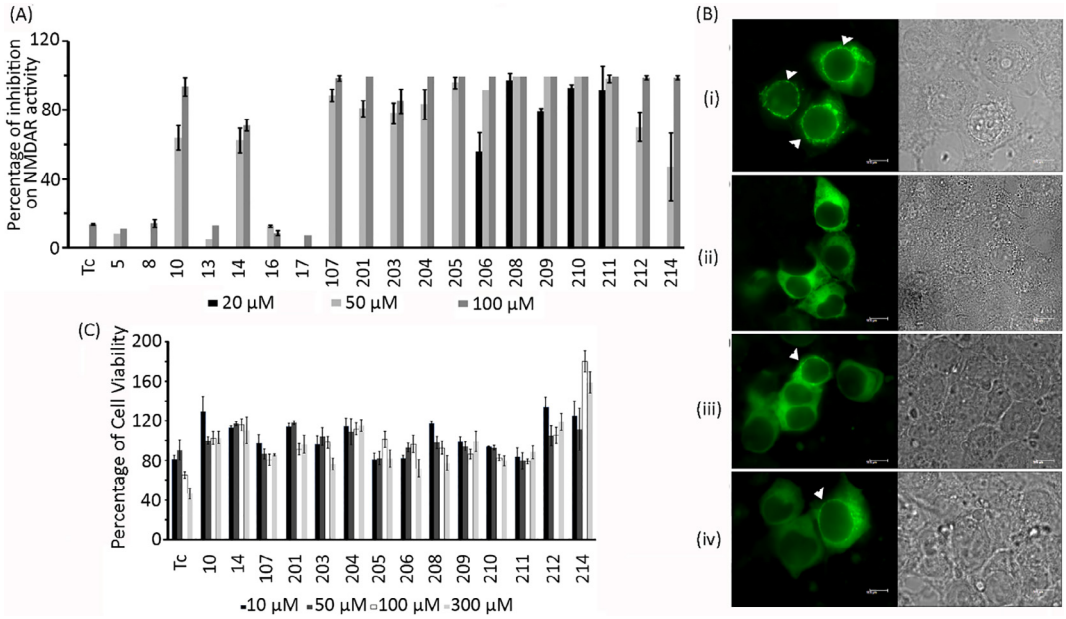

Fig. 2. *In vitro* inhibitory profile of MTDLs against NMDAR. (A) Initial screening of MTDLs and tacrine (Tc) for inhibition of NMDAR activity. The values presented are mean ± SD (n = 3). (B) Representative images of HEK-293 cells expressing GFP-α-CaMKII, GluN1 and GluN2B. (i) Punctate appearance in the presence of NMDAR agonists (glutamate and glycine) and calcium. (ii) Absence of punctate appearance in the presence of agonists but in the absence of Ca^{2+}; (iii) Reduction in the number of punctate cells when treated with NMDAR agonists, Ca^{2+} and 211 at 5 μM; (iv) Reduction in the number of punctate cells when treated with NMDAR agonists, Ca^{2+} and 208 at 5 μM. Right panel shows the corresponding bright field images. (C) Cytotoxicity of the compounds on HepG2 cell line (represented as mean ± SD, n = 3) after exposure for 24 h.

treatment. The extent of excitotoxic cell death was quantified biochemically by measuring the activity of glucose-6-phosphate dehydrogenase (G6PD) released into the medium (Fig. 3A). As expected, treatment with glutamate led to increased cell death which was prevented by the NMDAR inhibitor, MK-801. The results substantiated that cell death in this model is primarily mediated by NMDAR activation. Cell death was assessed by fluorescence imaging after immunostaining for the neuronal marker protein, microtubule associated protein 2 (MAP2) and also by observing chromatin condensation as detected by nuclear staining with DAPI (Fig. 3B). Immunocytochemical staining for MAP2, predominantly localized in dendrites [91] has been used as a marker to study neuronal integrity [92] and thus neuronal survival [93]. DAPI and immunostaining data showed a dramatic decrease in the viable and MAP2 positive neurons upon glutamate treatment. Staining experiments also showed that excitotoxicity induced by glutamate is prevented in the presence of MK-801. The percentage of viable cells and percentage of MAP2 positive neurons in the presence or absence of glutamate are shown in Fig. 3C. Glutamate mediated excitotoxicity was also checked using MTT assay 24 h after treating cultures with glutamate for 3 h. Compared to the glutamate free control, glutamate treatment showed a significant reduction in neuronal viability (Fig. 3D).

2.5.2. Treatment with tacrine derived MTDLs reduces glutamate induced toxicity

Based on the NMDAR inhibition pattern, our MTDLs can be classified into three categories of inhibitors such as potent (IC_{50} < 5 μM),

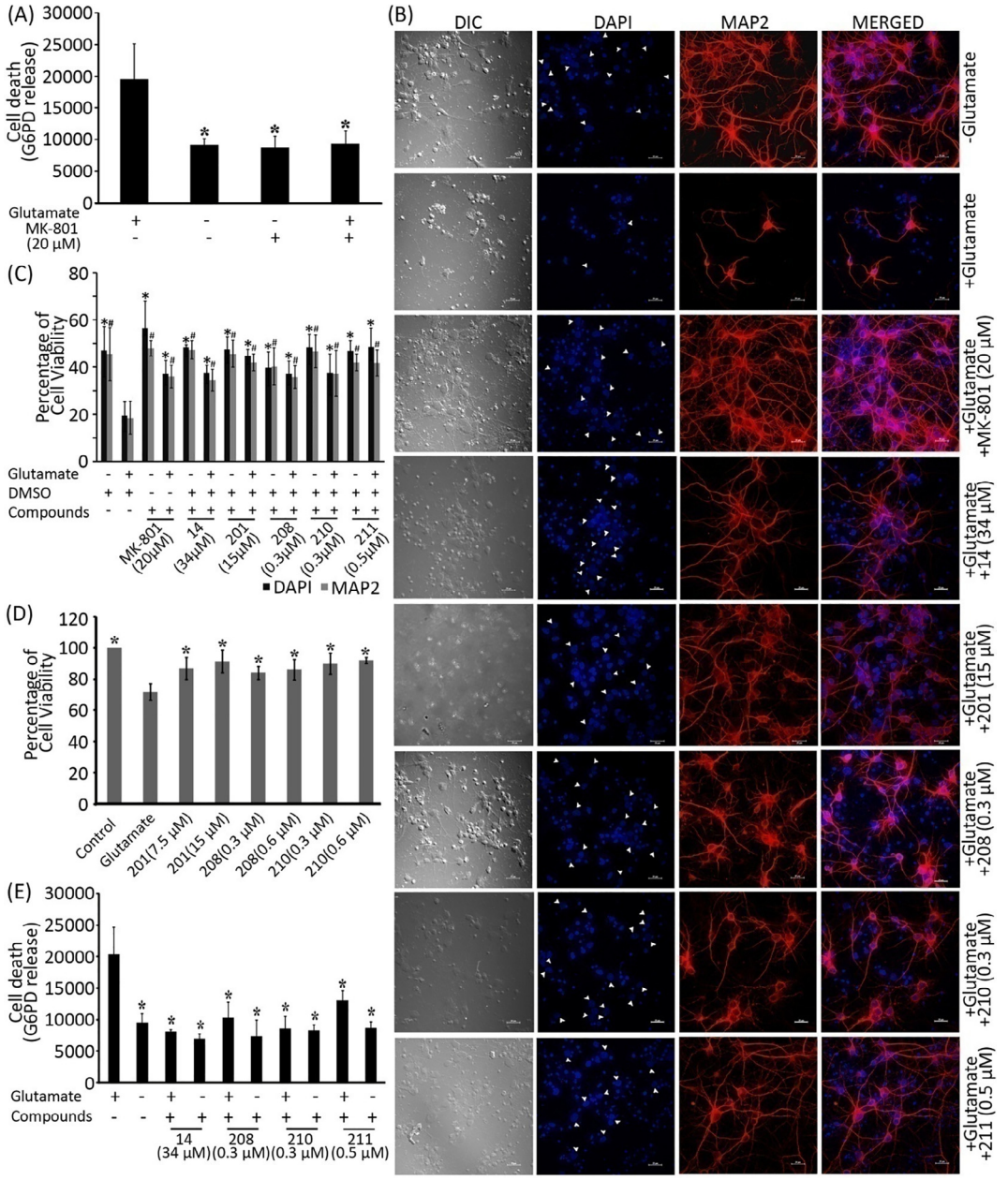

Fig. 3. Neuroprotective action of tacrine derived MTDLs on glutamate-induced excitotoxicity in primary cortical neurons on DIV9 treated with 100 μM glutamate and 10 μM glycine. (A) The extent of G6PD released as a part of excitotoxic cell death in the presence and absence of glutamate (represented as mean ± SD, n = 3), * indicates p value < 0.05 compared to glutamate treatment. (B) Representative images of primary cortical neurons immunostained for MAP2 (red) and counterstained with DAPI (blue) after treatment with 100 μM glutamate and 10 μM glycine in the absence or presence of MK-801 or selected tacrine derived MTDLs (14, 201, 208, 210 and 211). Live neurons are shown with arrow heads. (C) Quantification of glutamate-induced cell death detected by DAPI staining and MAP2 immuno-reactivity in cortical neurons. The bar diagrams represent the percentage of viable and MAP2 positive cells (represented as mean ± SD, n = 3). *and # indicates p value < 0.05 compared to glutamate treatment for viable cell count and MAP2 positive neurons respectively. (D) Glutamate induced neuronal death in the absence or presence of selected MTDLs (201, 208 and 210) measured using MTT assay (represented as mean ± SD, n = 3). * indicates p value < 0.05 compared to glutamate treatment. (E) Glutamate induced death of neurons in the absence or presence of selected MTDLs (14, 208, 210 and 211) measured using G6PD release assay (represented as mean ± SD, n = 3), DMSO was present in all samples. * indicates p < 0.05 compared to glutamate treatment. (For interpretation of the references to color in this figure legend, the reader is referred to the web version of this article.)

moderate (IC_{50} < 20 μM) and less potent (IC_{50} > 20 μM) ones. We selected candidates from each category to assess their neuroprotective properties. Totally five of the MTDLs (14, 201, 208, 210 and 211) were taken to assess their effects on glutamate induced excitotoxicity, of which three (208, 210 and 211) are potent blockers of NMDAR. The remaining two, 201 and 14, showed moderate and reduced potency towards NMDAR respectively. Biochemical assays such as G6PD release assay or MTT assay were performed to estimate the neuroprotective effect. All compounds were dissolved in DMSO (<0.05%) as it has been shown that DMSO does not have any protective effect against glutamate toxicity (Fig. S4). Controls with DMSO were used in all experiments.

Assays for G6PD release show that compounds 14, 208, 210 and 211 can protect neurons against glutamate toxicity at concentrations close to their respective IC_{50} values (Fig. 3E). The reduction in neuronal viability by glutamate treatment was averted in presence of compounds 201, 208 and 210 as evident from MTT assay. In these experiments, the neurons were treated with compounds along with glutamate after pre-treatment with compounds (Fig. 3D). Both the biochemical results clearly illustrate that these

compounds can protect cortical neurons from glutamate induced toxicity.

2.5.3. Treatment with tacrine derived MTDLs prevents glutamate induced neuronal injury

The protective effect of the compounds on glutamate-induced neuronal death was further studied by nuclear staining using DAPI. Glutamate treatment in the presence of compounds 14, 201, 208, 210 and 211 showed a clear decrease in the number of condensed nuclei compared to glutamate treatment in the absence of these compounds (Fig. 3B and C). This is an indication of neuroprotection by compounds against excitotoxicity.

2.5.4. Treatment with tacrine derived MTDLs prevents loss of neuronal integrity

The effect of MTDLs 14, 201, 208, 210 and 211 on glutamate induced loss of neuronal integrity was studied by immunocytochemical staining for MAP2. Decrease in MAP2 positive cells and loss of neuronal architecture caused by glutamate treatment were prevented in the presence of MTDLs, which pointed towards the protective role of these derivatives (Fig. 3B and C). No major changes were induced in neurons when treated with the compounds in the absence of glutamate (Fig. S4).

2.6. In vivo studies

2.6.1. Tacrine derived MTDLs ameliorated mono sodium glutamate (MSG) induced cognitive impairment

MSG has been shown to induce brain lesions and a series of behavioral disorders in various experiments by over-stimulating glutamate receptors [94–98]. Based on this information, MSG was used to achieve chronic excitotoxic conditions in a rat model to study neuronal damage-induced learning impairment using the MWM behavioral test. MSG (2 g/Kg body weight) was given intraperitoneally (IP) for 15 days. We selected tacrine, compounds 201 and 208 to assess whether these compounds can ameliorate MSG induced cognitive impairment. We administered these compounds by IP injection simultaneous to MSG treatment as described in the experimental section. The test included 3 days of training in the MWM. The mean escape latency values of all the groups on each day are shown in Fig. S5. Compared to saline treated group, MSG treated animals showed significant increase in latency to reach the platform on the 3rd day of trials (Fig. 4A) indicating impaired learning. The compounds 201 and 208 when administered along with MSG caused significant improvement in escape latency (Fig. 4A) showing that the compounds were able to ameliorate the impaired performance caused by administration of MSG. Simultaneous administrations of tacrine and MSG did not exhibit any significant improvement in learning ability when compared to MSG alone.

We further conducted experiments with the compound 201, to confirm its *in vivo* neuroprotective effect on learning and memory. Even though 201 has shown only moderate affinity towards NMDAR compared to 208, the non-toxic behavior of 201 on the HepG2 cell line compared to 208 encouraged us to select 201 for further studies. We used a higher dose of MSG i.e., 4 g/Kg body weight to induce excitotoxicity and the MWM test was conducted for 5 days. We found that latency to reach the platform for the MSG-treated group was significantly higher when compared to the control group upto 5 days (Fig. 4B). Treatment of 201 (3 mg/Kg body weight) along with MSG significantly reduced the escape latency compared to MSG alone, signifying that 201 could ameliorate the memory impairment caused even by a higher dose of MSG (Fig. 4C). The minor difference between the 201-saline and 201-MSG groups was not statistically significant. The representative trajectories of the trials are given in Fig. 4D.

2.6.2. MTDL-201 does not show in vivo hepatotoxicity

The animals treated with saline, tacrine, 201 or 208 as part of the *in vivo* behavioral analysis experiments were sacrificed by cervical dislocation after 15 days from start of injections. The fixed liver tissues were sectioned and were stained using Hematoxylin and Eosin (H&E). Treatment with 201 did not show any change in the liver architecture (Fig. 4E). Also, no fatty changes, necrosis or hepatic injury were observed. However, animals treated with 208 showed signs of hepatotoxicity such as mild periportal inflammation or mild congestion (in 5 out of 6 animals). Out of 6 animals of the tacrine treated group, one showed mild periportal inflammation or congestion. This clearly showed that 201 does not have hepatotoxic nature.

3. Discussion

Since 201 and 208 (differ only in the substitutions at the R4 position, where 201 and 208 have methylpyrazole and fluorobenzene moieties at the R4 position respectively) were promising candidates in most of the experiments, pharmacokinetic properties of these MTDLs were predicted using SwissADME and were compared with that of tacrine. The pharmacokinetic and pharmacodynamic properties of tacrine are already known [99] and served as a positive control in our molecular modeling studies.

The bioavailability radar plot enabled a first glance at the drug likeness of the compounds. Six physicochemical properties are considered: lipophilicity, size, polarity, solubility, flexibility and saturation. The physicochemical range on each axis is depicted as a colored zone in the radar plot, in which the molecules that fall entirely into the purple area are considered to be drug-like. The physicochemical properties of tacrine (Fig. 5A) and 201 (Fig. 5B) completely fall into the colored zone indicating their drug likeliness. The value of insaturation is slightly exceeding the recommended limit in the case of 208 (Fig. 5C). The tool also predicted that the compounds are blood–brain barrier (BBB) permeable. Since BBB is considered to be the bottleneck in CNS drug discovery, we have also checked the BBB permeability of the compounds by other online tools such as 'online BBB predictor' and QikProp (Schrödinger). Online BBB predictor was built by applying the support vector machine (SVM) and Ligand Classifier of Adaptively Boosting Ensemble Decision Stumps (LiCABEDS) algorithms [100] and was specially designed to classify compounds based on whether they can cross the BBB (BBB +) or not (BBB −). According to the tool, the threshold value for a compound to be BBB permeable is 0.02. The values predicted for tacrine, 201 and 208 are 0.120, 0.141 and 0.140 respectively indicating that all these compounds are BBB permeable (Fig. 5D). According to results obtained from QikProp, both 201 and 208 are BBB permeable and CNS active (Table S2).

Our docking studies revealed that both 201 and 208 can bind to AChE (Binding energy (ΔG) for 201 and 208 are −100 and −82 kcal/mol respectively) and NMDAR (ΔG for 201 and 208 are −80 and −82 kcal/mol respectively) much stronger than tacrine (ΔG for tacrine towards AChE and NMDAR are −79 and −68 kcal/mol respectively) (Fig. 5E). Both 201 and 208 bind to the active site of AChE and channel vestibule of NMDAR in a similar fashion as tacrine. We found that the tacrine moieties in 201 and 208 were well aligned to tacrine. The substitutions of methyl pyrazole in 201 and fluorophenyl in 208 favored stacking interactions with Y337 in AChE. Additionally, a hydrogen bond between hydroxyl group of Y341 and N atom of the pyrazole ring of 201 was observed (Fig. 5G). Both of these aromatic moieties improved the hydrophobic contacts with the surrounding residues. Binding modes of 201 and 208 at the channel vestibule of NMDAR are highly similar to each other; the substitutions on the tacrine moiety were oriented

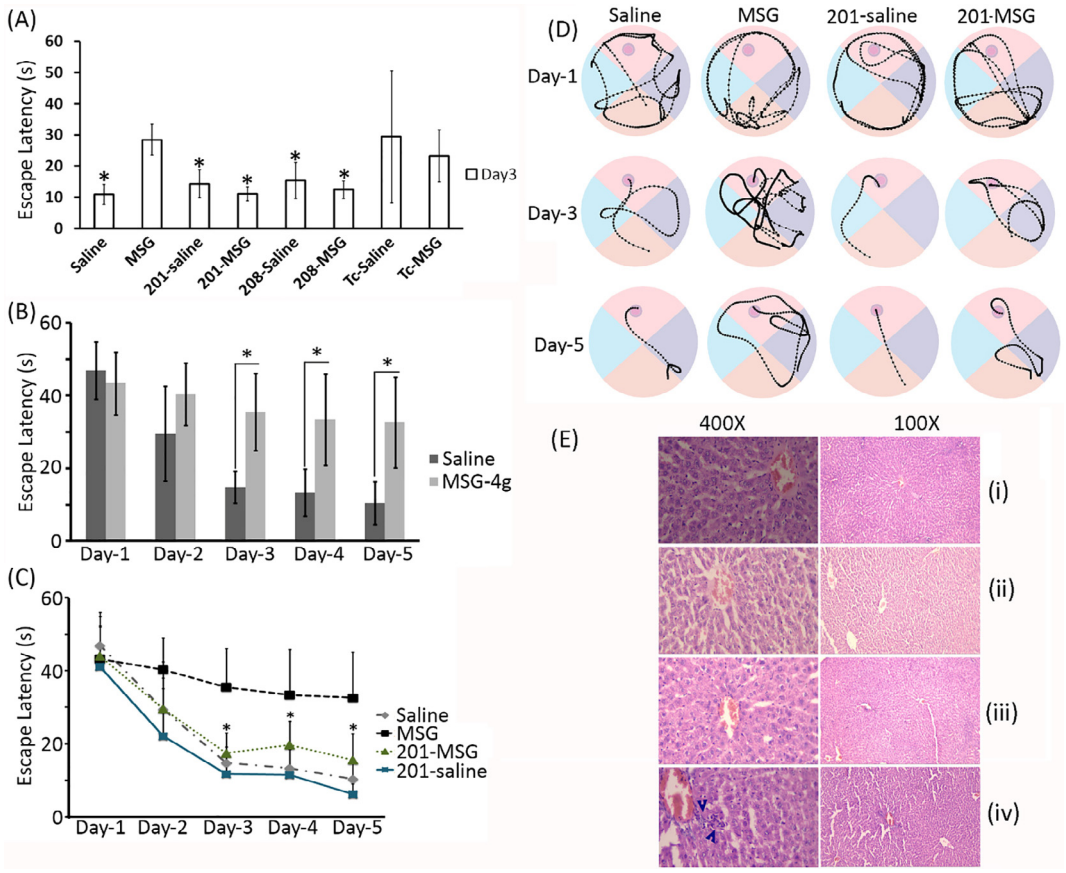

Fig. 4. The *in vivo* effect of selected MTDLs (201 and 208) assessed using MWM behavioral test and liver histopathology. Animals were subjected to treatment with saline or MSG along with the MTDL or vehicle. **(A)** Escape latencies of animals after the indicated treatments (represented as mean ± SD, n = 3) on 3rd day of trial, * indicates p value < 0.05 compared to treatment with MSG alone (2 g/Kg body weight). **(B)** Effect of higher dose of MSG (4 g/Kg body weight) on performance in learning and memory task compared to saline control. Escape latencies of the animals (represented as mean ± SD, n = 7) from Day1 to Day5 are shown, * indicates p value < 0.05 compared to corresponding saline of the same day. **(C)** Effect of compound-201 on cognitive impairment induced by MSG (4 g/Kg body weight). Escape latencies from Day1 to Day5 are shown (represented as mean ± SD, n = 7 for saline, MSG and 201-saline groups and n = 6 for 201-MSG group). * indicates p value < 0.05 compared to MSG treatment alone. The data for saline and MSG is same as that shown in B. **(D)** Representative trajectories of selected animals in each group in the MWM experiment on days 1, 3 and 5. (**E**) Liver histopathological analysis of animals treated with saline (i) (*n = 6*), tacrine (ii) (*n = 6*), compound-201 (iii) (*n = 7*) and compound-208 (iv) *(n = 6)* using Hematoxylin and Eosin staining (H&E).

between the M3 helices of GluN1 and GluN2B. The interactions of these compounds are largely favored by hydrophobic contacts with the residues in the M3 helices of both GluN1 and GluN2B (Fig. 5F). Since compounds 201 and 208 were promising and belong to group-2, we compared the *in vitro* inhibitory activities of other molecules in group-2 (Table 1). We found that aromatic or hetero aromatic ring substitutions at R4 position (201, 205, 208, 209, 211 and 212) favored the inhibitory activity against AChE and NMDAR. Also, halogen substitutions in the phenyl ring at R4 position favored inhibitory potency towards AChE and NMDAR (208 and 209). However, group-3 compounds that have substitutions at R1 and R4 positions (10 and 14) showed reduced inhibitory activity towards NMDAR and AChE. Although the group-1 compounds exhibited reduced inhibitory activity towards NMDAR, their binding towards AChE was promising. A simple schematic representation of the structure activity relationships (SAR) inferred based on the available data is shown in Fig. 5H.

We have been successful in improving the affinity of the designed MTDLs towards NMDAR without losing their potency towards AChE (Table 1). Indeed, AChE inhibitory activity was improved for some of the MTDLs (compounds 201, 203, 205, 208, 209, 212 and 214). The compounds 201, 204, 205, 208, 210, 212 and 214 also have submicromolar IC_{50} values against BChE. Molecular docking studies of these MTDLs against BChE (PDB ID:4BDS) reveals that they bind at the mid gorge of BChE and most of them make hydrogen bond with H438 and stacking interaction with W82. XP docking followed by MM-GBSA binding energy calculation was carried out to estimate the binding energy of the MTDLs against BChE. The binding energy of MTDLs towards BChE is shown in Table S3 and the binding mode of the MTDLs at the active site gorge of BChE is shown in Figure S6. There is substantial evidence suggesting that BChE plays an important role in regulating ACh levels in the later stages of AD [101–105]. Hence the inhibition of BChE is also highly desirable in addition to AChE inhibitory activity and compound 208 has displayed comparable inhibitory potency towards both AChE and BChE.

The MTDLs 203, 205 and 211 exhibited slight toxicity in HepG2 cells (Fig. 2C), but they are comparatively better than tacrine. These MTDLs also exhibited more potency towards AChE and NMDAR when compared to tacrine. Hence, we assume that these compounds would be effective in inhibiting their targets at lower doses than tacrine and thereby may have lesser hepatotoxicity under *in vivo* conditions. Indeed 201 did not show hepatotoxicity in its efficacious dose in the animal model. Although 208, the other MTDL that was tested *in vivo*, showed hepatotoxicity at the dose used (Fig. 4E), it may be possible to find lower efficacious doses of the compound at which hepatotoxicity could be eliminated.

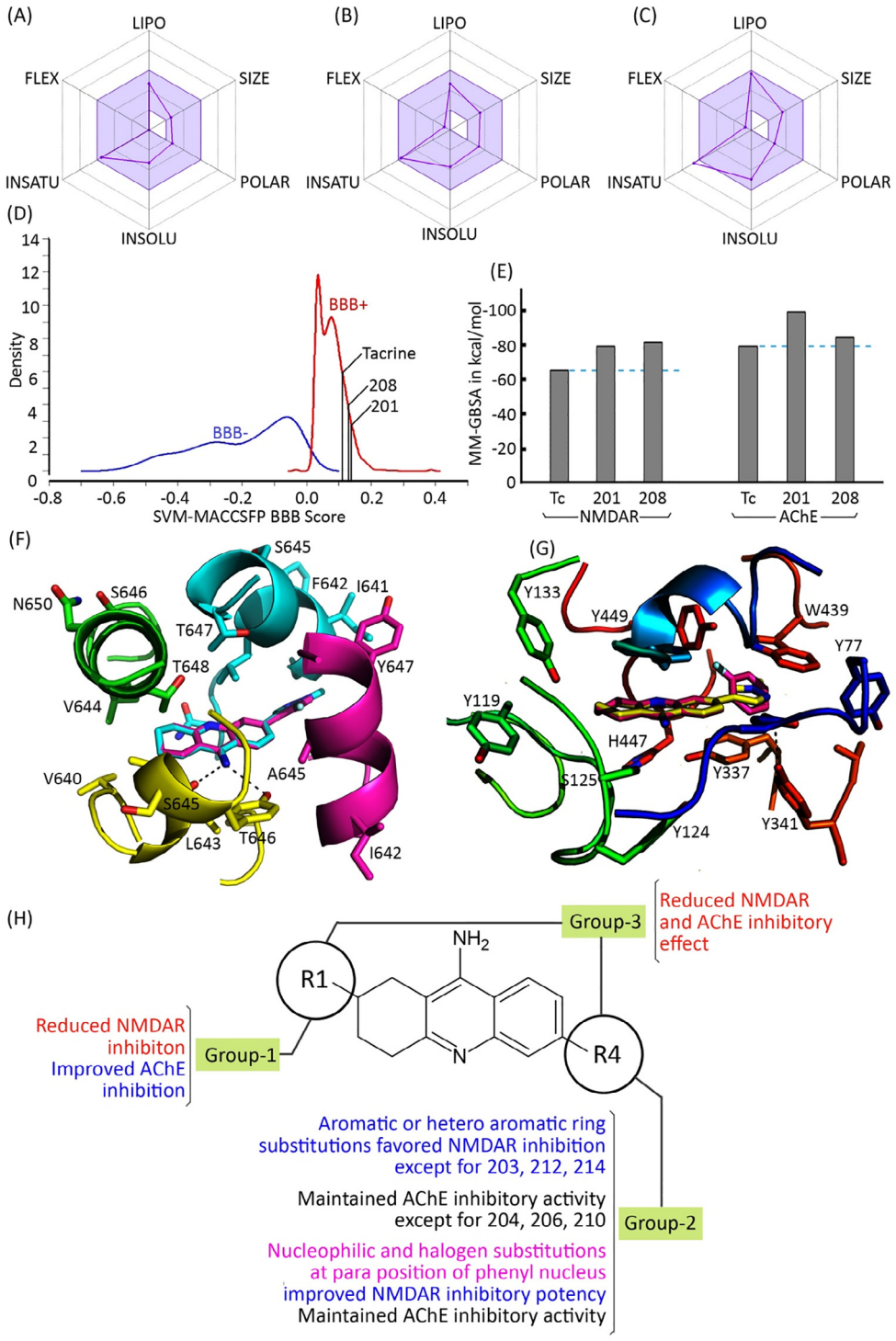

Fig. 5. *In silico* ADME properties, binding mode and binding energies determined for tacrine and selected tacrine derived MTDLs 201 and 208. Oral bioavailability radar plots of tacrine (A), 201 (B) and 208 (C), predicted using SwissADME are shown, in which the colored zone represents the suitable physico-chemical space for oral bioavailability. The optimum range of these properties are as follows: LIPO (Lipophilicity): −7.0 < XLOGP3<+5.0; SIZE:150 g/mol < MW < 500 g/mol; POLAR (Polarity): 20 Å^2 < TPSA < 130 Å^2; INSOLU (Insolubility): 0 < Log S (ESOL) < 6; INSATU (Insaturation): 0.25 < Fraction Csp3 < 1; FLEX (Flexibility): 0 < No. of rotatable bonds < 9. (D) Blood brain barrier permeability predicted using 'online BBB predictor'. The values (SVM-MACCSFP BBB score) predicted for tacrine, 201 and 208 are 0.120, 0.141 and 0.140 respectively. Reference ranges of SVM-MACCSFP BBB score for training set with (marked in red) and without (marked in blue) BBB penetrability are also shown. All compounds are predicted to be BBB+. (E) The binding energies calculated for tacrine, 201 and 208 against h-NMDAR and human AChE using Prime MM-GBSA method. (F) Binding modes of 201 (cyan stick) and 208 (purple stick) in the channel vestibule of modeled h-NMDAR (cartoon representation). (G) Binding modes of 201 (yellow stick) and 208 (purple stick) at the active site gorge of human AChE (cartoon representation). Hydrogen bonds are shown as dotted lines in both (F) and (G). (H) Structure vs activity relationship of the synthesized molecules. (For interpretation of the references to color in this figure legend, the reader is referred to the web version of this article.)

Our MTDLs reported in the current study are more potent than other FDA approved AChEI such as rivastigmine (IC_{50} = 4.15 μM) [14] and galantamine (IC_{50} = 15.06 μM) [106]. Hence, we believe that at reduced doses of these MTDLs, they could still be therapeutically effective. Moreover, increase in the efficacy of NMDAR inhibition could contribute to the multi targeting effect to achieve

overall therapeutic outcome. Hence, we expect that the MTDLs reported in the current study will be beneficial for the treatment of AD as they can act on multiple pathways that underlie cognitive decline and neuronal loss towards achieving disease modification.

Although the etiology varies among different neurodegenerative diseases, neuronal injury and subsequent neuronal death is common. This is primarily caused by excessive activation of NMDAR and hence NMDAR antagonists might be useful in various neurodegenerative conditions. We also expect that these MTDLs would be beneficial in acute conditions such as ischemia [35], stroke [36] and TBI [37] in which NMDAR hyperactivity causes significant damage. In acute conditions, since the NMDAR antagonists are used for relatively shorter duration, the risk of side effects would be lesser and hence higher doses might be permissible. Our biochemical and cytological investigations revealed that glutamate induced excitotoxicity and the consequent death of neurons in culture were prevented by MTDLs such as 14, 201, 208, 210 and 211. Also, these compounds were neuroprotective (Fig. 3B) at the concentration at which they showed effective inhibition of heterologously expressed NMDAR (Table 1) indicating that their mechanism of neuroprotection might be driven by NMDAR inhibition.

Additionally, the *in vivo* neuroprotection studies of 201 and 208 indicated that they can effectively rescue brain function from MSG mediated impairment. Although 201 is a moderate inhibitor of NMDAR compared to 208, it was efficient in neuroprotection both *in vivo* and *in vitro*. Previous studies demonstrated the neuroprotective properties of aryl azoles and have shown that methyl pyrazole moiety can favor neuroprotective property [107]. Hence, we presume that methyl-pyrazole moiety also might have contributed to the neuroprotective property of 201 apart from NMDAR inhibition. The neuroprotective action of 208 might be solely related to NMDAR inhibition since it is a potent NMDAR antagonist.

MSG has been shown to induce brain lesions and behavioral impairments in various experiments by overactivating glutamate receptors [94–98]. The MSG treatment protocol that we have used, created a model of excitotoxic stress of a subacute and chronic nature. We believe the protection offered by 201 and 208 in the MSG treated rats could be the result of the NMDAR inhibitory activities of these compounds. While the *in vivo* efficacy of these compounds needs to be tested in more animal models of cholinergic and/or glutamatergic deficiencies, our data show that the newly designed MTDLs are indeed acting in the animal model as predicted by modeling and *in vitro* studies.

4. Conclusion

Due to the multifactorial etiology of neuropsychiatric diseases, MTDLs have been suggested as better disease modifying agents than single target directed drugs. It is widely accepted that these MTDLs not only can earnestly ameliorate the symptoms but also modify the disease. Tacrine, the first approved drug for AD, had hepatotoxicity. In spite of this, tacrine moiety has served as a template for the designing of hybrids and MTDLs. Though tacrine has been reported to be a potent AChE inhibitor and weak NMDAR antagonist, its binding mode was unknown. In this study, we demonstrated the binding modes of tacrine towards AChE and NMDAR through molecular modeling. With an aim to design potential MTDLs against AChE and NMDAR, we rationally designed 75 tacrine derivatives based on the predicted binding mode of tacrine. Among them, 19 molecules were chemically synthesized and were evaluated *in vitro* against both of these targets. We found that the derivatization improved AChE inhibitory potential for few compounds like, 13, 17, 201, 203, 205, 208, 209, 211, 212 and 214. The derivatization also improved the antagonistic potential towards NMDAR for compounds like 10, 14, 107, 201, 203, 204, 205, 206, 208, 209, 210, 211, 212 and 214. Based on the inhibition data, we tried to generate an SAR for the designed compounds. We found that substitutions at R1 and R4 positions together, reduce NMDAR and AChE inhibitory activity. Aromatic/hetero aromatic substitutions at R4 position of tacrine are key determinants for improved antagonistic potential towards NMDAR. These SAR would be useful for future discovery of potent tacrine derived MTDLs. The preliminary assessment of cytotoxic nature of the MTDLs on HepG2 cell line suggested that derivatization lowered the toxic nature of the compounds when compared to the parent compound, tacrine. A few MTDLs were tested for their effect on rat primary cortical neurons subjected to glutamate induced excitotoxicity and were found to be neuroprotective. Further, *in vivo* studies of the selected tacrine derived MTDLs, 201 and 208, using a rat model of MSG induced excitotoxicity showed that these compounds were able to protect the animals against MSG induced behavioral impairment thus demonstrating their efficacy *in vivo*. Our *in silico* ADME predictions of 201 and 208 suggested that they are drug like molecules with promising therapeutic and acceptable pharmacokinetic properties thus encouraging further *in vivo* studies. The *in vivo* hepatotoxicity assessment showed that 201 is non hepatotoxic in nature although 208 showed mild hepatotoxicity at the dose used. Based on the entire study, we suggest that the tacrine derived MTDL, 201 is a potential drug candidate for further evaluation *in vivo* while the other derivatives need more *in vitro* and *in vivo* investigations.

5. Materials and methods

5.1. Computational approaches

5.1.1. Modeling of NMDAR, structure-based design of tacrine derivatives and their ensemble docking towards NMDAR and AChE

Extensive molecular modeling studies were performed to model h-NMDAR, to understand the binding mode of tacrine towards AChE and NMDAR, to design tacrine derived MTDLs and to predict the binding affinity of the designed inhibitors against NMDAR and AChE.

5.1.2. Coarse-grained modeling of NMDAR

Crystal structure of GluN1/GluN2B delta-ATD NMDAR from *Xenopus laevis* in complex with MK-801 (NMDAR antagonist) (PDB ID: 5UN1) [108] was used for our modeling studies. Since, MK-801 is an NMDAR antagonist, its binding site in the pore was taken as the spatial reference for the docking of tacrine. Initially, the missing regions in GluN1/GluN2B were patched and mutations were replaced with original h-NMDAR amino acids using structure prediction wizard of Schrödinger. We employed an extensive loop refinement to optimize the newly constructed regions. A systematic coarse-grained modeling using NMA and ENM was performed on the modeled structure to address the structural dynamics of NMDAR. Programs such as Phenix SCEDS, Bio3D, Schrödinger and web servers such as WEBnma and iMod were used for the NMA and elNémo was used for ENM [109–113]. Majority of the programs except Phenix SCEDS provided multiple output structures in the form of polyalanine C-alpha traces. Amino acid backbone structures were built from the C-alpha traces by optimizing the main chain hydrogen-bonding networks using REMO algorithm [114]. Finally, polyalanine-independent conformational conversion of these structures was performed using the 'Mutate residue range' option using Coot. All output structures were clustered based on the global RMSD and one candidate structure was chosen from each of the clusters and was prepared for ensemble docking.

5.1.3. Preparations of tacrine and tacrine derived MTDLs for docking studies

Compounds such as tacrine and its derivatives were prepared using LigPrep module, Schrödinger and were used for molecular docking. LigPrep produced energy-minimized and protonated structures at pH 7.0 ± 2 with different ionization states, tautomerism, stereoisomerism and ring conformations. Optimized potential for liquid simulations (OPLS3) force field was used for energy minimization of the ligand structures [115].

5.1.4. Ensemble docking of tacrine with NMDAR

Prior to ensemble docking, the candidate receptor structures were prepared using protein preparation wizard of Schrödinger. During the preparation, hydrogen atoms were added to the polar groups, bond orders were corrected and a short energy minimization was performed with an RMSD cutoff of 0.30 Å using OPLS-3 force field. By specifying the spatial reference of MK-801, a grid of size 20 Å was prepared on the four ensemble structures. The size of the grid was designed in such a way that it will cover the whole channel and hence all possible binding sites in the channel. Finally, the prepared ligands were docked in the grid using standard precision and induced fit docking method.

5.1.5. Ensemble docking of tacrine with AChE

In order to understand how multiple conformations of AChE affect the binding of tacrine and its derivatives, ensemble docking was carried out. Four different human AChE (hAChE) structures were taken for docking studies. These structures differ in the conformation of an active site residue, Y337. Out of four structures, one was the apo structure (PDB ID: 4EY4) [78] and the others were in complex with donepezil (PDB ID:4EY7) [78], huperzine (PDB ID:4EY5) [78] and 9-aminoacridine (PDB ID:6O4X) [116]. These hAChE structures were prepared for docking as described above after removing the crystallographic water molecules.

5.1.6. Structure based designing of tacrine derivatives, ensemble docking towards NMDAR and AChE and their binding energy calculations

In order to design MTDLs, the lowest energy receptor bound conformation of tacrine was used. Previous studies which explained the binding modes of different tacrine derivatives against AChE [55] also served as potential references for designing MTDLs. We generated several tacrine derived MTDLs using a rational design approach by taking into consideration the conformations of residues surrounding the bound tacrine. Standard precision and induced fit docking method was used to predict the binding mode of the designed ligands towards both targets. After docking, the binding energy was estimated for each ligand complex using prime MM-GBSA method and structure activity relationships were deduced computationally.

5.1.7. Prediction of ADME properties

For computational assessment of absorption, distribution, metabolism and excretion (ADME) properties of the compounds, we calculated physico-chemical parameters of the selected MTDLs using QikProp, Schrödinger and SwissADME [117]. Parameters important for CNS activity and blood–brain barrier (BBB) permeability were mainly assessed for selected molecules using QikProp, SwissADME and online BBB predictor [118].

5.2. Chemical synthesis

In order to validate our *in silico* findings, promising MTDLs were chemically synthesized. All experiments were set-up on fume hoods and were carried out under nitrogen atmosphere in Schlenk tubes, unless otherwise stated. All solvents and reagents were procured from commercially available sources like Sigma-Aldrich, Combi-Blocks and Spectrochem. Commercially available prepacked silica gel (230–400 mesh) plugs were used for column chromatography. All of the synthesized molecules were purified using solvents such as hexane, ethyl acetate, dichloromethane and methanol. Isolated yields correspond to products of > 95% purity for the synthesized compounds as determined by LC-MS and NMR. ^{1}H NMR was recorded on Bruker 400 MHz AVANCE series or Bruker 300 MHz DPX Spectrometer with CD_3OD or DMSO-D_6 as the solvent. All NMR chemical shifts were reported in parts per million (ppm), all coupling constants were reported in Hertz (Hz) and tetramethylsilane was used as internal standard for ^{1}H NMR. Multiplicities are abbreviated as follows: singlet (s), doublet (d), triplet (t), quartet (q), doublet–doublet (dd), multiplet (m), and broad (br). Liquid chromatography-mass spectrometry (LC-MS) was used for reaction monitoring and determination of product mass on Agilent 1100 Series LC/MSD mass spectrometer. The compound numbers shown in parenthesis (Table S1) indicate the compound numbering according to our patent application (IPO-201841015699).

5.2.1. General procedure for the synthesis of 6-bromo-1,2,3,4-tetrahydroacridin-9-amine (Compound 3)

To a solution of 2-amino-4-cyano-benzonitrile (1) (5.0 g, 0.0253 mol, 1.0 equiv) in anhydrous toluene was added boron trifluoride etherate (3.76 mL, 0.0304 mol, 1.2 equiv) slowly at room temperature. The reaction mixture was cooled to 0 °C followed by the addition of cyclohexanone (2) (3.9 mL, 0.0379, 1.5 equiv) and the reaction mixture was heated to 100 °C for 4 h. After completion of reaction as monitored by TLC, the reaction mixture was quenched with aq.NaOH solution upto pH = 10 and the reaction mixture was diluted with ethyl acetate. The organic layers were separated, dried over sodium sulphate and concentrated. The crude product was recrystallized from dichloromethane to obtain 6-bromo-1,2,3,4-tetrahydroacridin-9-amine (3) (5.8 g, 82%) as pale-yellow solid. ^{1}H NMR: DMSO d_6 (400 MHz): δ 8.13 (d, 1H, J = 8.8 Hz), 7.81 (s, 1H), 7.40–7.37 (m, 1H), 6.50 (bs, 2H), 2.82–2.79 (m, 2H), 2.55–2.52 (m, 2H), 1.82–1.80 (m, 4H).^{13}C NMR (100 MHz, dmso) δ 172.15, 157.30, 149.89, 145.28, 127.81, 125.99, 124.55, 122.30, 115.36, 109.61, 32.34, 23.42, 22.06, 21.17; LC-MS: m/z 279.0 (M + 2), Analysis calculated for $C_{13}H_{13}BrN_2$.

5.2.2. General procedure for the synthesis of 9-amino-6-(1-methyl-1H-pyrazol-4-yl)-1,2,3,4-tetrahydroacridinium (Compound 201)

To a solution of 6-bromo-1,2,3,4-tetrahydroacridin-9-amine (3) (100 mg, 0.36 mmol, 1.0 equiv) in 1,4-dioxane (4 mL) and water (0.5 mL) were added 1-methyl pyrazole 4-boronic ester (4a) (90 mg, 0.434 mmol, 1.2 equiv) and sodium carbonate (57 mg, 0.54 mmol, 1.5 equiv). The reaction mixture was degassed for 10 min and $Pd(PPh_3)_4$ (41.0 mg, 0.036 mmol, 0.1 equiv) was added. The reaction mixture was heated to 110 °C for 2 h in a sealed tube. The reaction mixture was filtered through celite, washed with ethyl acetate (50 mL). The filtrate was diluted with water (50 mL) and extracted by ethyl acetate (3 × 50 mL). The organic layers separated were dried over anhydrous sodium sulphate and were concentrated under vacuum. The crude product was purified by column chromatography using 10% methanol in dichloromethane as eluent to give 6-(1-methyl-1H-pyrazol-4-yl)-1,2,3,4-tetrahydroacridin-9-amine (Compound 201) (50 mg, 50% yield) as an off white solid.^{1}H NMR: NMR: MoD (400 MHz): δ 8.13–8.10 (m, 2H), 7.97 (s, 1H), 7.81 (s, 1H), 7.66 (dd, 2H, J = 8.4, 1.6 Hz), 3.98 (s, 3H), 2.97–2.94 (m, 2H), 2.65–2.62 (m, 2H), 1.97–1.95 (m, 4H); ^{13}C NMR (101 MHz, dmso) δ 154.70, 151.14, 142.81, 136.53, 134.29, 128.67, 123.21, 121.89, 121.05, 114.21, 108.64, 23.11,

21.88, 21.71; LC-MS: *m*/*z* 279.1 (M + 1), Analysis calculated for $C_{17}H_{18}N_4$.

5.2.3. 6-(pyrimidin-5-yl)-1,2,3,4-tetrahydroacridin-9-amine (Compound 203):

Compound 203 was synthesized in a similar way as 201 but using pyrimidin-5-ylboronic acid (4b) (54 mg, 0.434 mmol, 1.2 equiv) instead of 4a; Yield: 55 mg, 55%; ^{1}H NMR: MeOD (400 MHz): δ 9.18 (s, 3H), 8.22–8.20 (m, 1H), 8.00 (m, 1H), 7.69–7.66 (dd, 1H, *J* = 8.8, 1.8 Hz), 2.97–2.94 (m, 2H), 2.66–2.63 (m, 2H), 1.96–1.93 (m, 4H); ^{13}C NMR (100 MHz, dmso) δ 158.33, 157.26, 154.83, 147.97, 146.61, 132.94, 132.90, 126.00, 123.34, 120.83, 116.99, 109.57, 63.18, 33.59, 32.64, 23.74, 22.59, 22.47; LC-MS: *m*/*z* 277.2 (M + 1), Analysis calculated for $C_{17}H_{16}N_4$.

5.2.4. 6-(1H-pyrazol-3-yl)-1,2,3,4-tetrahydroacridin-9-amine (Compound 204)

Compound 204 was synthesized in a similar way as 201 but using (1H-pyrazol-3-yl) boronic acid (4c) (49 mg, 0.434 mmol, 1.2 equiv) instead of 4a; Yield: 48 mg, 50%; ^{1}H NMR: MeOD (400 MHz): δ 8.10–8.05 (m, 2H), 7.82–7.79 (m, 1H), 7.71 (m, 2H), 6.81(d, 1H, *J* = 2.0 Hz), 2.96–2.93 (m, 2H), 2.66–2.63 (m, 2H), 1.95–1.90 (m, 4H); ^{13}C NMR (100 MHz, tfa) δ 155.06, 153.67, 145.18, 136.46, 134.67, 129.09, 123.63, 123.53, 116.84, 115.20, 111.12, 106.28, 27.71, 21.02, 19.90, 19.37; LC-MS: *m*/*z* 265.2 (M + 1), Analysis calculated for $C_{16}H_{16}N_4$.

5.2.5. 4-(9-amino-5,6,7,8-tetrahydroacridin-3-yl)benzonitrile (Compound 205)

Compound 205 was synthesized in a similar way as 201 but using (4-cyanophenyl) boronic acid (4d) (64 mg, 0.434 mmol, 1.2 equiv) instead of 4a; Yield: 60 mg, 55%; ^{1}H NMR: DMSO (300 MHz): δ 8.29–8.26 (m, 2H), 8.19–8.16 (m, 1H), 8.00–7.99 (m, 1H), 7.86–7.83 (m, 1H), 7.72–7.67 (m, 2H), 6.44 (bs, 2H), 2.90–2.80 (m, 2H), 2.72–2.68 (m, 2H), 1.90–1.87 (m, 4H); ^{13}C NMR (100 MHz, dmso) δ 155.52, 151.47, 142.64, 136.95, 134.77, 132.89, 131.29, 127.72, 121.76, 119.90, 114.96, 110.50, 109.51, 27.76, 22.60, 20.99, 20.47, 3.61; LC-MS: *m*/*z* 300.2 (M + 1), Analysis calculated for $C_{20}H_{17}N_3$.

5.2.6. 6-(4-(trifluoromethoxy)phenyl)-1,2,3,4-tetrahydroacridin-9-amine (Compound 206)

Compound 206 was synthesized in a similar way as 201 but using (4-(trifluoromethoxy)phenyl) boronic acid (4e) (90 mg, 0.434 mmol, 1.2 equiv) instead of 4a; Yield: 59 mg, 45%; ^{1}H NMR: MeOD (400 MHz): δ 8.17 (d, 1H, *J* = 8.8 Hz), 7.96–7.94 (m, 1H), 7.86–7.84 (dd, 2H, *J* = 6.4, 2.0 Hz), 7.69–7.66 (dd, 1H, *J* = 4.8, 2.0 Hz), 7.43–7.41 (m, 2H), 2.98–2.95 (m, 2H), 2.67–2.64 (m, 2H), 2.01–1.90 (m, 4H); ^{13}C NMR (100 MHz, dmso) δ 157.80, 148.29, 147.92, 146.22, 139.10, 138.04, 128.73, 125.08, 122.99, 121.47, 116.35, 109.23, 33.33, 23.65, 22.53, 22.44; LC-MS: *m*/*z* 359.0 (M + 1), Analysis calculated for $C_{20}H_{17}F_3N_2O$.

5.2.7. 6-(2-fluorophenyl)-1,2,3,4-tetrahydroacridin-9-amine (Compound 208)

Compound 208 was synthesized in a similar way as 201 but using (2-fluorophenyl) boronic acid (4g) (61 mg, 0.434 mmol, 1.2 equiv) instead of 4a; Yield: 63 mg, 60%; ^{1}H NMR: MeOD (400 MHz): δ 8.42 (d, 1H, *J* = 8.8 Hz), 7.94 (s, 1H), 7.94–7.80 (m, 1H), 7.67–7.72 (m, 1H), 7.60-0.7.49 (m, 1H), 7.40–7.37 (m, 1H), 7.37–7.25 (m, 1H), 3.05–3.02 (m, 2H), 2.68–2.65 (m, 2H), 2.03–1.98 (m, 4H); ^{13}C NMR (100 MHz, dmso) δ 167.07, 160.47, 148.38, 146.04, 134.34, 130.92, 129.66, 128.11, 125.03, 123.24, 122.41, 116.86, 116.31, 116.09, 113.69, 34.52, 32.63, 32.60, 27.66, 22.22, 20.77 LC-MS: *m*/*z* 293.2 (M + 1), Analysis calculated for $C_{19}H_{17}FN_2$.

5.2.8. 6-(4-fluorophenyl)-1,2,3,4-tetrahydroacridin-9-amine (Compound 209)

Compound 209 was synthesized in a similar way as 201 but using 2-(4-fluorophenyl)-4,4,5,5-tetramethyl 1,3,-dioxaborolane (4h) (96 mg, 0.434 mmol, 1.2 equiv) instead of 4a; Yield 72 mg, 68%; ^{1}H NMR: MeOD (400 MHz): δ 8.37 (d, 1H, *J* = 8.4 Hz), 7.87–7.81 (m, 2H), 7.79–7.77 (m, 2H), 7.70–7.61 (m, 1H), 7.58–7.55 (m, 1H), 7.29–7.24 (m, 2H), 3.03–3.02 (m, 2H), 2.63–2.61 (m, 2H), 2.05–1.90 (m, 4H); ^{13}C NMR (100 MHz, dmso) δ 155.11, 151.63, 137.40, 131.34, 130.04, 129.50, 124.29, 123.19, 119.92, 116.88, 116.68, 116.27, 114.10, 27.78, 22.57, 21.01, 20.48; LC-MS: *m*/*z* 293.2 (M + 1), Analysis calculated for $C_{19}H_{17}FN_2$.

5.2.9. 6-(4-(methylthio)phenyl)-1,2,3,4-tetrahydroacridin-9-amine (compound 210)

Compound 210 was synthesized in a similar way as 201 but using 4,4,5,5-tetramethyl-2-(4-(methylthio) phenyl)-1,3,2-dioxaborolane (4i) (109 mg, 0.434 mmol, 12 equiv) instead of 4a; Yield: 64 mg, 55%; ^{1}H NMR: MeOD (400 MHz): δ 8.39 (d, 1H, *J* = 8.0 Hz), 7.91 (m, 2H), 7.43 (d, 2H, J = 8.8), 7.42 (d, 2H, J = 8.8), 3.05–3.02 (m, 2H), 2.67–2.64 (m, 2H), 2.56 (s, 3H), 2.01–2.00 (m, 4H); ^{13}C NMR (100 MHz, dmso) δ 155.14, 143.81, 138.67, 137.55, 127.44, 126.30, 124.03, 115.24, 109.12, 32.67, 32.61, 27.79, 21.04, 14.38; LC-MS: *m*/*z* 312.2 (M + 1), Analysis calculated for $C_{20}H_{20}N_2S$.

5.2.10. 6-(4-(trifluoromethyl)phenyl)-1,2,3,4-tetrahydroacridin-9-amine (Compound 211)

Compound 211 was synthesized in a similar way as 201 but using (4-(trifluoromethyl)phenyl) boronic acid (4j) (83 mg, 0.434 mmol, 1.2 equiv) instead of 4a; Yield: 75 mg, 61%; ^{1}H NMR: MeOD (400 MHz) δ 8.47 (d, 1H, *J* = 8.8 Hz), 8.01–7.92 (m, 4H), 7.88–7.86 (m, 2H), 3.10–3.06 (m, 2H), 2.72–2.65 (m, 2H), 2.10–1.99 (m, 4H); ^{13}C NMR (100 MHz, dmso) δ 155.05, 151.67, 142.13, 142.02, 137.34, 128.85, 127.96, 126.07, 124.47, 124.27, 116.63, 114.32, 109.34, 27.75, 22.59, 20.99, 20.46; LC-MS: *m*/*z* 343.0 (M + 1), Analysis calculated for $C_{20}H_{17}F_3N_2$.

5.2.11. 6-(furan-3-yl)-1,2,3,4-tetrahydroacridin-9-amine (compound 212)

Compound 212 was synthesized in a similar way as 201 but using 2-(furan-3-yl)-4,4,5,5-tetramethyl-1,3,2-dioxaborolane (4k) (84 mg, 0.434 mmol, 1.2 equiv) instead of 4a; Yield: 35 mg, 37%; ^{1}H NMR: MeOD (400 MHz): δ 8.33 (d, 1H, *J* = 8.8 Hz), 8.21 (s, 1H), 7.87–7.81 (m, 2H), 7.65–7.55 (m, 2H), 3.04–3.01 (m, 2H), 2.66–2.63 (m, 2H), 2.03–1.99 (m, 4H); ^{13}C NMR (100 MHz, dmso) δ 155.10, 151.30, 145.24, 141.67, 137.69, 136.25, 131.51, 128.81, 124.13, 123.53, 113.95, 109.09, 108.35, 27.73, 22.52, 21.02, 20.50; LC-MS: *m*/*z* 265.2 (M + 1), Analysis calculated for $C_{17}H_{16}N_2O$.

5.2.12. 6-(pyridin-3-yl)-1,2,3,4-tetrahydroacridin-9-amine (Compound 214)

Compound 214 was synthesized in a similar way as 201 but using 3-(4,4,5,5-tetramethyl-1,3,2- dioxaborolan-2-yl)pyridine (4m) (89 mg, 0.434 mmol, 1.2 equiv) instead of 4a; ^{1}H NMR: MeOD (400 Hz): 9.44 (s, 1H), 9.14 (d, 1H, *J* = 8.0 Hz), 9.01 (d, 1H, *J* = 6.4 Hz), 8.62 (d, 1H, *J* = 8.8 Hz), 8.31 (m, 1H), 8.24 (s, 1H), 8.09 (d, 1H, *J* = 8.8 Hz), 3.11–3.09 (m, 2H), 2.70–2.67 (m, 2H), 2.03–2.02 (m, 4H); ^{13}C NMR (100 MHz, dmso) δ 155.15, 152.00, 139.00, 137.34, 131.52, 131.42, 128.71, 126.16, 124.74, 124.32, 117.11, 114.71, 109.68, 27.49, 22.64, 20.99; LC-MS: *m*/*z* 276.0 (M + 1), Analysis calculated for $C_{18}H_{17}N_3$.

5.2.13. General procedure for the synthesis of ethyl 9-amino-1,2,3,4-tetrahydroacridine-2-carboxylate (compound 16)

To a solution of 2-amino benzonitrile (1a) (5.0 g, 0.0253 mol, 1.0 equiv) in anhydrous toluene was added boron trifluoride etherate (3.76 mL, 0.0304 mol, 1.2 equiv) slowly at room temperature. The reaction mixture was cooled to 0 °C followed by the addition of ethyl-4-oxocyclohexanecarboxylate (2a) (6.4 mL, 0.0379 mol, 1.5 equiv) and the reaction mixture was heated to 100 °C for 4 h. After completion of reaction as monitored by TLC, the reaction mixture was quenched with aqueous sodium hydroxide solution at pH = 10 and the reaction mixture was diluted with ethyl acetate. The organic layers were separated, dried over sodium sulphate and concentrated. The crude product was recrystallized from dichloromethane to obtain ethyl 9-amino-1,2,3,4-tetrahydroacridine-2-carboxylate (Compound 16) (7.0 g, 85%) as an off-white solid [55]. ^{1}H NMR (300 MHz, DMSO d_6): δ 8.14 (d, 1H, J = 8.37 Hz), 7.61 (d, 1H, J = 8.31 Hz), 7.48 (t, 1H, J = 6.9 Hz), 7.27 (t, 1H, J = 6.93 Hz), 6.43 (s, 2H), 4.18–4.08 (m, 2H), 2.87–2.82 (m, 4H), 2.72–2.62 (m, 1H), 2.26e2.12 (m, 1H), 1.88e1.82 (m, 1H), 1.23 (t, 3H, J = 7.11 Hz); ^{13}C NMR (100 MHz, dmso) δ 175.88, 163.05, 146.98, 133.19, 127.20, 116.62, 114.50, 67.27, 39.08, 35.44, 32.59, 23.01; LC-MS: m/z calculated for $C_{16}H_{18}N_2O_2$: 270.33; Observed mass: 271.2 (M + H).

5.2.14. Ethyl 9-amino-6-bromo-1,2,3,4-tetrahydroacridine-2-carboxylate (Compound 5)

Compound 5 was synthesized in a similar way as 16 but using 4-bromo-2-amino benzonitrile. ^{1}H NMR (400 MHz, DMSO d_6): δ 8.13 (d, 1H, J = 8.96 Hz), 7.79 (s, 1H), 7.40 (dd, 1H, J = 8.92, 8.92 Hz), 6.61 (s, 2H), 4.19–4.07 (m, 2H), 2.94–2.85 (m, 4H), 2.68–2.61 (m, 1H), 2.15–2.11 (m, 1H), 1.89–1.80 (m, 1H), 1.24 (t, 3H, J = 7.12 Hz); ^{13}C NMR (100 MHz, dmso) δ 174.66, 157.69, 148.57, 147.46, 129.69, 125.44, 124.33, 121.38, 115.79, 107.69, 60.09, 32.11, 26.12, 25.17, 14.16; LC-MS: 351.7 (M + 2), m/z calculated for $C_{16}H_{17}BrN_2O_2$.

5.2.15. General procedure for the synthesis of Ethyl-9-amino-6-(1-methyl-1H-pyrazol-4-yl)-1,2,3,4-tetrahydroacridine-2-carboxylate (Compound 10)

To a solution of ethyl 9-amino-6-bromo-1,2,3,4-tetrahydroacridine-2-carboxylate (5) (1.0 g, 2.87 mmol) in 1,4-dioxane (10 mL) and water (1 mL), 1-methyl pyrazole 4-boronic ester (4a) (0.9 g, 4.31 mmol) and sodium carbonate (0.6 g, 5.74 mmol) were added. The reaction mixture was degassed for 10 min and $Pd(PPh_3)_4$ (0.33 g, 0.287 mmol) was added. The reaction mixture was heated to 110 °C for 2 h in a sealed tube. The reaction mixture was filtered through celite, the filtrate was diluted with water (200 mL) and was extracted with ethyl acetate (3x200 mL). The organic layers separated were dried over anhydrous sodium sulphate and were concentrated under vacuum. The residue obtained was recrystallized in dichloromethane to afford compound 10 (0.52 g, 52%) as a white solid [55]. ^{1}H NMR (400 MHz, DMSO d_6): δ 8.26 (s, 1H), 8.16 (d, J = 8.0 Hz, 1H), 7.99 (m, 1H), 7.82 (m, 1H),7.55 (m, 1H), 6.57 (bs, 2H), 4.15 (m, 2H), 3.89 (s, 3H), 2.88 (m, 4H), 2.69 (m, 1H), 2.16 (m, 1H), 1.90 (m, 1H), 1.26 (t, J = 7.12, 3H); ^{13}C NMR (100 MHz, dmso) δ 174.74, 136.37, 128.25, 122.59, 121.66, 120.97, 106.64, 81.35, 60.08, 26.07, 25.24, 24.95, 24.48, 14.17; LC-MS:336.2 (M + H) m/z calculated for $C_{19}H_{21}N_5O$.

5.2.16. Synthesis of ethyl 9-amino-6-(4-fluorophenyl)-1,2,3,4-tetrahydroacridine-2-carboxylate (compound 107)

Compound 107 was synthesized in a similar way as 10 but using 2-(4-fluorophenyl)-4,4,5,5-tetramethyl-1,3,2 dioxaborolane (4h); ^{1}H NMR (400 MHz, MeOD): δ 8.14 (d, J = 8.8 Hz, 1H), 7.91 (m, 1H), 7.80–7.75 (m, 2H), 7.58 (dd, J = 8.0, 2.0 Hz, 1H), 7.24 (m, 2H), 4.22 (m, 2H), 3.05–3.01 (m, 2H), 2.99–2.90 (m, 2H), 2.89–2.82 (m, 1H), 2.33–2.29 (m, 1H), 2.6–1.98 (m, 1H), 1.32 (t, J = 7.2 Hz, 3H); ^{13}C NMR (100 MHz, tfa) δ 177.31, 155.68, 150.51, 146.98, 137.65, 128.70, 128.61, 126.32, 121.86, 118.41, 115.87, 115.59, 113.24, 112.78, 109.96, 63.30, 38.45, 26.72, 23.60, 22.64, 11.98; LC-MS: 365.2 (M + H) m/z calculated for $C_{22}H_{21}FN_2O_2$.

5.2.17. General procedure for the synthesis of 9-Amino-N-methyl-6-bromo-1,2,3,4-tetrahydroacridine-2-carboxamide (Compound 13)

To a solution of compound 5 (100 mg, 0.37 mmol) in methanol (4 mL) aq. ammonia (1 mL) was added and the reaction mixture was heated to 60 °C for 2 h. The reaction mixture was concentrated to dryness and was recrystallized from dichloromethane to give compound 13 [55]. White solid; Yield 80 mg, 80%; ^{1}H NMR (400 MHz, DMSO d_6): $\boldsymbol{\delta}$ 8.15–8.12 (m, 1H), 7.94 (d, J = 4.4 Hz, 1H), 7.81 (m, 1H), 7.42 (d, J = 8.8 Hz, 1H), 6.68 (bs, 3H), 2.88 (s, 3H), 2.76–2.68 (m, 3H), 2.15–2.12 (m, 1H), 2.01–1.98 (m, 1H), 1.91–1.81 (m, 2H); ^{13}C NMR (100 MHz, dmso) δ 176.33, 174.92, 157.48, 148.88, 129.19, 125.58, 124.36, 121.61, 115.63, 108.38, 32.40, 31.93, 27.02, 26.14, 25.81, 25.57; LC-MS: m/z calculated for $C_{15}H_{17}N_3O$: 225.14; Observed mass: 226.2 (M + H).

5.2.18. 9-amino-N-methyl-6-(1-methyl-1H-pyrazol-4-yl)-1,2,3,4-tetrahydroacridine-2-carboxamide (Compound 14)

Compound 14 was synthesized in a similar way as 13 but using compound 10; Yield: 50 mg, 92 % as a white solid. ^{1}H NMR (400 MHz, DMSO d_6): δ 8.37 (s, 1H), 8.16 (d, J = 8.4 Hz, 1H), 7.99 (s, 1H), 7.95 (m, 1H), 7.81 (s, 1H), 7.56 (d, J = 8.0 Hz, 1H), 6.67 (bs, 2H), 3.89 (s, 3H), 2.89 (m, 2H), 2.60 (m, 4H), 2.33 (m, 1H), 2.15 (m, 1H), 1.91 (m, 1H), 1.81 (s, 1H); ^{13}C NMR (100 MHz, dmso) δ 175.88, 163.05, 146.98, 133.19, 127.20, 116.62, 114.50, 67.27, 39.08, 35.44, 32.59, 23.01; LC-MS: 351.4 (M + H) m/z calculated for $C_{20}H_{22}N_4O_2$.

5.2.19. General procedure for the synthesis of 9-amino-1,2,3,4-tetrahydroacridine-2-carbohydrazide (compound 17)

To a solution of compound 16 (100 mg, 0.37 mmol) in methanol (4 mL), hydrazine hydrate (1 mL) was added and the reaction mixture was refluxed for 3 h at 70 °C. The reaction mixture was concentrated and was recrystallized from dichloromethane to give compound 17 [55]. Brown solid; Yield 80 mg, 85%;^{1}H NMR (400 MHz, MeOD): δ 8.28–8.20 (m, 1H), 7.82–7.80 (m, 1H), 7.74–7.71 (m, 1H), 7.69–7.58 (m, 1H), 3.09–3.03 (m, 2H), 2.91–2.80 (m, 3H), 2.26–2.22 (m, 1H), 2.06–2.03 (m, 1H); ^{13}C NMR (100 MHz, tfa) δ 179.62, 155.64, 136.69, 134.03, 126.80, 120.93, 118.39, 118.32, 118.23, 115.50, 115.41, 112.68, 112.60, 109.87, 109.78, 106.58, 37.54, 26.36, 23.13; LC-MS: m/z calculated for $C_{14}H_{16}N_4O$: 256.13; Observed mass: 257.2 (M + H).

5.2.20. 9-Amino-6-bromo-1,2,3,4-tetrahydroacridine-2-carbohydrazide (compound 8)

Compound 8 was synthesized in a similar way as 17 but using compound 5; White solid; Yield 70 mg, 73%; ^{1}H NMR (400 MHz, DMSO d_6): δ 8.15 (s, 1H), 8.11(d, J = 8.8 Hz, 1H), 7.79 (d, J = 2.0 Hz, 1H), 7.40–7.37 (m, 1H), 6.56 (s, 2H), 4.24 (bs, 2H), 2.91–2.77 (m, 2H), 2.72–2.67 (m, 2H), 1.96 (m,1H), 1.83 (m, 1H); ^{13}C NMR (100 MHz, dmso) δ 174.00, 157.14, 147.57, 145.04, 131.01, 130.24, 124.30, 118.28, 115.42, 108.50, 32.63, 26.93, 25.92; LC-MS: m/z calculated for $C_{14}H_{15}BrN_4O$: 334.04; Observed mass: 336.2 (M + 2).

5.3. In vitro studies

To understand the pharmacological properties of the synthesized MTDLs, we performed *in vitro* activity assays of cholinesterases and NMDAR.

5.3.1. In vitro cholinesterase (AChE and BChE) inhibition assays

Enzymatic assays for AChE were carried out in a 96-well plate using AMPLITE™ AChE assay kit (AAT Bioquest, Inc., Sunnyvale, CA, USA) which consists of AChE from *Electrophorus electricus* (electric eel) (structural similarity towards human AChE is ≥ 90 %) [119,120], assay buffer (pH 7.4), 5,5-dithiobis-(2-nitrobenzoic acid) (DTNB, known as Ellman's reagent) and the substrate acetylthiocholine (AChT). The assay system works on the basis of Ellman's method [121]. Thiocholine, produced by the action of AChE on acetylthiocholine, forms a yellow-colored product with DTNB. The quantity of the colored product measured at 410 ± 5 nm, is proportional to enzyme activity. The native enzyme reaction was carried out by mixing enzyme (0.3U) with 125 μM AChT (in ddH_2O) and 125 μM DTNB (in assay buffer). The same experiment was repeated in the presence of the selected MTDLs. The MTDLs, were dissolved in 0.01 % DMSO and were pre-incubated with AChE at room temperature for 20 min prior to the addition of reaction mixture containing AChT and DTNB. The OD at 405 nm of the reaction mixture in the presence and absence of compounds was plotted against time and from there the relative activity of the enzyme in the presence of compounds was calculated. The half maximal inhibitory concentration (IC_{50}) was determined for the MTDLs by performing the assay at different inhibitor concentrations.

The inhibitory effect of all the compounds against butyrylcholinesterase (BChE) was also determined in a similar way. In this experiment, BChE from equine serum (0.3 U), butyrylthiocholine (500 μM) and DTNB (500 μM) in PBS (pH 7.4) were used for the inhibition assays. In all the experiments, the IC_{50} values are presented as the mean ± standard deviation of at least three separate experiments.

5.3.2. Effect of MTDLs on NMDA receptor activity

To check the effect of MTDLs on NMDAR activity a cell-based assay system was used which works via protein–protein interaction between NMDAR and α-CaMKII [82]. The plasmids coding for NMDAR subunits, GluN1 and GluN2B, and α-CaMKII tagged with GFP (GFP-α-CaMKII) were co-transfected into HEK-293 cells and the activity of GluN2B containing NMDAR was detected. In order to perform the assay, following procedures were performed.

5.3.2.1. Preparation and transfection of plasmids coding for GluN1, GluN2B and GFP-α-CaMKII to HEK-293 cells. The plasmids for mammalian expression carrying the cDNAs for GluN1, GluN2B and GFP-α-CaMKII were prepared from bacterial cells using QIAGEN Midi Kit (Qiagen, USA). The plasmids were quantified using NanoDrop 2000 and their purity was checked on 1% agarose gel as reported previously [82]. These plasmids were further co-transfected into pre-grown HEK-293 cells using lipofectamine (Invitrogen) according to the manufacturer's protocol (quantities of the plasmids per well used for transfection: GluN1 and GluN2B – 0.35 μg each and GFP-α-CaMKII – 0.15 μg). HEK-293 cells were grown by seeding them on sterile 12 mm coverslips placed in 24-well plates (~1.5 × 10^4 cells/well). About 18 h after seeding, the cells were co-transfected with the plasmids. Upon terminating the transfection reaction after 5 h with 20% fetal bovine serum (FBS) in Dulbecco's modified Eagle's medium (DMEM), 20 μM MK-801 was also added. The addition of MK-801 prevented cell death in transfected cells that can happen due to activation of NMDAR. The transfection solution was aspirated after 12 h and 500 μL of fresh DMEM containing 10% FBS and 20 μM MK-801 was added. The cells were further incubated at 37 °C for 24 h.

5.3.2.2. NMDAR activity assay. About 24 h after transfection, cells were washed twice, first with Hank's balanced salt solution (HBSS) containing 1 mM HEPES and 0.5 mM EGTA (Solution I) and then with HBSS containing 1 mM HEPES (Solution II). NMDAR was activated with Solution III [solution II containing NMDAR agonists, glutamate (100 μM) and glycine (10 μM), along with Ca^{2+} (2 mM)]. After 5 min of activation, cells were fixed with 4% paraformaldehyde (PFA) for 10–15 min and were washed thrice with PBS. The cover slip containing cells were mounted on a clean glass slide using glycerol: PBS (1:1) and were visualized using a fluorescence microscope. The activity of GluN2B containing NMDAR was detected based on translocation of GFP-α-CaMKII to GluN2B subunit in the endoplasmic reticulum (ER), nuclear membrane and plasma membrane. It was observed as redistribution of green fluorescence accumulation (punctae) at the membranes. To check the effect of MTDLs on NMDAR activity, the compounds at respective concentrations were included in both solution II (pre-incubation for 5 min) and solution III. In order to quantitate NMDAR activity, the cells were counted using a fluorescence microscope (Leica DMI 4000B inverted microscope) at 40X magnification. The number of green fluorescent cells and green fluorescent cells with punctae were counted separately and the percentage of green fluorescent cells having a punctate pattern was calculated as [(number of punctate cells /total number of green fluorescent cells) × 100]. This number was taken as the efficiency of punctae formation or punctate cell count. For each slide, 5 or more fields were randomly selected and the average of punctate cell count for all the fields was estimated. Further, percent inhibition of activity in presence of the compounds with respect to the control was calculated. Final values were obtained from three independent experiments. For IC_{50} measurements, each estimation was done with 6 or more concentrations of the MTDLs. IC_{50} values from three such determinations were used to calculate mean ± SD for each compound.

5.3.2.3. Effect of MTDLs on interaction between GFP-α-CaMKII and GluN2B. In order to study the effect of MTDLs on the interaction of GFP-α-CaMKII and GluN2B, HEK-293 cells stably expressing GFP-α-CaMKII and a construct having the GluN2B motif which binds to α-CaMKII, tagged with mitochondrial localization signal (MLS-NR2B) was used [82]. Since there are no functional NMDAR channels in the membrane, GFP-α-CaMKII was activated by Ca^{2+} influx through ionomycin, a Ca^{2+} ionophore. The activated GFP-α-CaMKII binds to MLS-NR2B and the interaction can result in the formation of perinuclear punctae of green fluorescence. To achieve this, cells grown on the coverslips were first washed with HBSS containing 1 mM HEPES and 0.5 mM EGTA for 5 min. Subsequently the cells were incubated with 250 μL HBSS containing 1 mM HEPES and 15 μM ionomycin with or without MTDL for 5 min. Next, the cells were treated with HBSS containing 1 mM HEPES, 2 mM Ca^{2+} and 3 μM ionomycin with or without MTDL for 5 min. The cells were fixed using 4% PFA for 10 min and were washed twice with PBS for 5 min each. The coverslips were mounted onto glass slides and were used for imaging. Concentrations of the MTDLs which exhibited ≥ 70% inhibition of NMDAR activity were chosen for further studies.

5.3.3. Cell viability and neuroprotection studies

To understand the toxicity profile of MTDLs, we have estimated their effect on the viability of HepG2 cells using MTT assay. The neuroprotective property of selected MTDLs against glutamate induced excitotoxicity was performed in primary rat cortical neuronal cells.

5.3.4. In vitro assay for checking the toxicity of MTDLs on HepG2 cells

In the MTT assay, the live cells are estimated by the reduction of MTT (pale yellow) into dark purple formazan crystals by the action of mitochondrial succinate dehydrogenase, which is monitored using spectrophotometer by measuring absorbance at 570 nm. Initially the HepG2 cells were maintained in DMEM supplemented

with 10% FBS, 10,000 units/mL penicillin, 10 mg/mL streptomycin and 25 μg/mL amphotericin-B in T-25 flasks. Cells were trypsinized using 0.25% trypsin and were seeded onto 96-well plates (~15000 cells/well). After 24 h, the medium was aspirated and was replaced with fresh medium containing varying concentrations of the selected MTDLs (10, 50, 100 and 300 μM). After growing the cells for 24 h, 5 mg/mL MTT solution was added to the cells and was kept for an additional 2 h. The formazan crystals formed were dissolved in 100 μL DMSO and absorbance at 570 nm was measured using a multimode plate reader (Infinite® 200 from TECAN). Cell viability is expressed as the percentage of viable cells compared to untreated cells.

5.4. Experiments in primary neuronal cultures

5.4.1. Preparation of primary cortical neurons from E18 rat embryos

Primary cultures of cortical neurons were prepared from Wistar rat embryos at E18 stage. All animal studies were carried out at Rajiv Gandhi Centre for Biotechnology (RGCB), Thiruvananthapuram, according to the Institutional Animal Ethics Committee guidelines. The pregnant female rat was sacrificed, the uterus was carefully removed with the embryos and was placed in a 90 mm petri dish containing ice cold phosphate-buffered saline (PBS). Embryos were then removed from the uterus and the brain was dissected from each embryo. The cortical hemispheres were separated and the meninges were removed with the help of a stereo microscope. The tissues were minced gently in HBSS and were centrifuged at 345*g* for 3 min. The tissue was then dissociated using 0.05% Trypsin-EDTA and DNase I (4000 U/mL) for 10 min. Action of trypsin on the tissue was arrested by addition of 10% FBS, followed by a wash with HBSS and centrifugation at 345*g* for 3 min. Tissues were triturated to a single cell suspension using DMEM containing DNase I (4000 U/mL) and were washed twice with DMEM by centrifugation at 345*g* for 5 min. Live cells were counted using trypan blue dye exclusion method and the cells were then seeded onto 24-well plates and 96-well plates, pre-coated with poly-D-lysine (100 μg/mL) and laminin (1 μg/mL), at a density of 1×10^5 cells/well and 20×10^3 cells/well respectively, in neurobasal medium (NBM) supplemented with 1X GlutaMAX, 1X antibiotic/antimycotic solution, 1X B27 supplement and ciprofloxacin (10 μg/mL). The plates were incubated at 37 °C under 5% CO_2. The cells were maintained in culture, by changing the media at regular intervals, till the day of experiment.

5.4.2. Induction of excitotoxicity in primary cortical neurons using glutamate

Glutamate-induced excitotoxicity was performed on primary cortical neurons that were maintained for nine days *in vitro* (DIV9). Prior to the experiment, the cells were washed with solution I (HBSS, 10 mM HEPES, pH 7.4 and 0.2 mM EGTA) for 10 min followed by treatment with solution II (HBSS, 10 mM HEPES, pH 7.4) for 10 min. Subsequently, these cells were incubated with solution III (HBSS, 10 mM HEPES, pH 7.4, 100 μM glutamate, 10 μM glycine, 1.2 mM $CaCl_2$) for 60 min for induction of excitotoxicity. To check the activity of MTDLs, the compounds were included in solution II and III. MK-801 (20 μM) was used as a positive control in these experiments. After 60 min of glutamate treatment, solution III was replaced with NBM and the cells were maintained for 24 h. The spent media was used for biochemical estimation of G6PD release and the cells were utilized for immunocytochemistry and DAPI staining by fixing them using 4% PFA. The cortical cells grown in 96-well plates were subjected to MTT assay after excitotoxicity treatment, which is explained in the section **'MTT assay for measuring neuronal death'**.

5.4.3. Glucose 6-phosphate dehydrogenase assay for measuring neuronal death

Since the damaged cells release G6PD to the surrounding medium, we quantified G6PD using Vybrant™ cytotoxicity assay kit (Molecular Probes) and measured neuronal death. The assay kit utilizes the generated NADPH to reduce resazurin to red fluorescent resorufin (Abs/Em: 563/587 nm) by the action of diaphorase enzyme. The resulting fluorescence intensity is proportional to the amount of G6PD released into the medium which correlates with cell death. After excitotoxicity treatment, 50 μL of spent media was mixed with 50 μL of the reagent in a 96-well plate, incubated at 37 °C for 40 min and fluorescence emission was measured at 587 nm. All necessary experimental controls and samples were assayed in duplicate.

5.4.4. MTT assay for measuring neuronal death

The cortical neurons subjected to excitotoxic treatments at DIV9 stage were subjected to MTT assay. Excitotoxicity was induced as explained in the section 'Induction of excitotoxicity in primary cortical neurons using glutamate' except that glutamate treatment was given for 3 h and the treatment solutions were replaced with NBM. The cells were maintained for another 24 h and MTT assay was carried out as explained in the section '*In vitro* assay for checking the toxicity of MTDLs on HepG2 cells'.

5.4.5. Immuno and DAPI staining of primary cortical neurons

Immunostaining was carried out to visualize the distribution and localization of the neuronal marker protein, microtubule associated protein (MAP2) during excitotoxic conditions and DAPI was used as a nuclear counterstain. Cells after excitotoxicity treatment were fixed with PFA, washed thrice with PBS and were permeabilized and blocked simultaneously with PBS containing 0.2% triton X-100 and 3% BSA for 1 h at room temperature. After removing the blocking solution, the cells were incubated with the primary antibody [MAP2 antibody – 1:1000] diluted in PBS containing 2% BSA and 0.3% triton X-100 overnight at 4 ^{0}C. The primary antibody was then removed and the cells were washed thrice with PBS followed by incubation with secondary antibody conjugated to Cy3 at a dilution of 1:500, for 1–2 h at room temperature. The cells were washed thrice with PBS before being stained with DAPI (1.8 μM) for 20 min at room temperature. The cells were again washed thrice with PBS and the coverslips were mounted using fluoromount and were sealed with DPX. The slides were viewed using an epifluorescence microscope (Leica DMI 6000B inverted microscope) and the images were captured at 40X magnification. The percentage of viable cells and total number of cells were calculated from the DAPI stained nuclei in each field and percentage of MAP2 positive cells (calculation performed by counting MAP2 stained cells upon total number of DAPI stained cells in each field) were also calculated. All treatments were done in duplicates for each experiment. Values obtained from 10 fields were averaged for each experiment. DMSO treatment was included as a control.

5.5. Behavioral analysis using Morris water maze test

To understand the effect of MTDLs on *in vivo* excitotoxicity, we induced excitotoxic condition in rats by administering MSG. The treatment is expected to affect cognitive behavior of rats which was assessed using the MWM behavioral test. The performance in the test was compared between control rats and rats subjected to treatment of MTDLs. The experimental procedure is as follows.

Studies were conducted using 4–6 weeks old, male Wistar rats (~100 g). MSG solutions were administered IP for 15 days. Every rat received two injections each day, an initial injection of the selected MTDL or vehicle followed by saline or MSG (2–4 g/Kg body weight) in saline 30–45 min later. The MWM test was started on the 11th

day of treatment, as described by Morris [122], with a slight modification. The water maze apparatus consisted of a large circular pool (183 cm diameter, 64 cm height), with an escape platform (10 cm diameter, 35 cm height) and was filled with milky water to a level just above the platform. The rat was placed into the water, facing the tank wall (starting point) and was allowed to search for the platform for 60 s (maximum trial time allowed) based on the visual cues present in the room. The trajectories of the rat were recorded using a video camera with EthoVision XT software (Noldus Information Technology). The time taken by each rat to reach the platform (escape latency) was measured using the software. If the rat finds the platform before 60 s, it was allowed to stay on the platform for 5–10 s and was then returned to its home cage. On the other hand, if the rat was unable to find the platform, it was physically placed on the platform for 10 s and then was returned to its home cage. Each animal was given five trials per day (11th to 15th day of injections) with an interval of ~ 10–15 s between each trial. For the initial screening of MTDLs, the rats were divided into the following groups, with three rats in each group (n = 3): (i) Vehicle control (0.03% DMSO in saline), (ii) MSG (2 g/Kg body weight), (iii) compound 201 (3 mg/Kg body weight) control, (iv) compound 201 (3 mg/Kg body weight) and MSG, (v) compound 208 (1 mg/Kg body weight) control, (vi) compound 208 (1 mg/Kg body weight) and MSG, (vii) tacrine (5 mg/Kg body weight) control and (viii) tacrine (5 mg/Kg body weight) and MSG. For subsequent confirmatory studies, the dose of MSG administered was 4 g/Kg body weight and the n value was raised to at least 6.

5.6. In vivo hepatotoxicity assessment using histopathology

The animals used for the behavioral studies mentioned in the previous section were sacrificed by cervical dislocation, the livers were dissected carefully and were fixed in 10% buffered formalin. Each treatment group that received a compound or vehicle as the first injection, included animals that received saline or MSG as the second injection. Histopathology of the fixed liver samples was carried out by outsourcing to a clinical histopathology lab. The procedure used was as follows: the liver lobe was embedded in paraffin block and 5 μm sections were prepared. The sections were further deparaffinated and were stained with H&E. After staining, slides were prepared and were viewed under bright field compound binocular research microscope at 100X and 400X. Histological parameters for inflammation and toxicity were assessed visually by a pathologist and the samples were graded accordingly.

5.7. Statistical analysis

Statistical analysis of data obtained from *in vitro* and *in vivo* experiments was done using one way ANOVA followed by Tukey's post hoc test using Origin Pro 8 software. The significance level was set at $p < 0.05$. The quantitated values were represented as graphs with mean ± standard deviation (SD).

6. Associated content

Additional tables and figures are given in the Supporting Information.

CRediT authorship contribution statement

Chandran Remya: Conceptualization, Data curation, Formal analysis, Investigation, Methodology, Software, Validation, Visualisation, writing original draft, writing-review and editing. **K.V. Dileep:** Conceptualization, Data curation, Formal analysis, Methodology, Software, Validation, Visualisation, writing original draft, writing-review and editing. **Eeda Koti Reddy:** Data curation, Formal analysis, Investigation, Methodology, Validation, Visualisation, writing original draft, writing-review and editing. **Kumar Mantosh:** Formal analysis, Investigation, Methodology, Validation, Visualisation, writing-review and editing. **Kesavan Lakshmi:** Investigation, Methodology, Writing-review and editing. **Reena Sarah Jacob:** Investigation, Methodology, writing-review and editing. **Ayyiliyath M Sajith:** Methodology, writing - review and editing. **E.Jayadevi Variyar:** Conceptualization, Project administration, Resources, Supervision, Writing-review and editing. **Shaik Anwar:** Data curation, Formal analysis, Funding acquisition, Project administration, Resources, Supervision, Validation, Visualisation, Writing-review and editing. **Kam Y. J. Zhang:** Project administration, Resources, Supervision, Writing-review and editing. **C. Sadasivan:** Conceptualization, Project administration, Resources, Supervision, Writing-review and editing. **R. V. Omkumar:** Conceptualization, Funding acquisition, Project administration, Resources, Supervision, Validation, Visualisation, Writing-review and editing

Declaration of Competing Interest

The authors declare that they have no known competing financial interests or personal relationships that could have appeared to influence the work reported in this paper. C.R., E.K.R., E.J.V., S. A., C.S. and R.V.O. are inventors of patent application containing data presented in this manuscript.

Acknowledgements

C.R., K.V.D, M.K, L.K and R.S.J acknowledge the fellowships received from Indian Council of Medical Research (ICMR) (No. BIC/11(48)/2012), Japan Society for the Promotion of Science (JSPS) (No. 16F16385), Kerala State Council for Science Technology and Environment (KSCSTE) (No. 03/FSHP/2013/CSTE), Council of Scientific and Industrial Research (CSIR) (No. 09/716(0153)/2013-EMR-I) and Department of Science and Technology (DST) (No. IF150638) respectively. S.A gratefully acknowledges DST-SERB for financial support under Young Scientist Scheme (SB/FT/CS-079/2014). Research funding received by RVO from Rajiv Gandhi Centre for Biotechnology, Thiruvananthapuram is also acknowledged. We gratefully acknowledge RIKEN ACCC for the supercomputing resources at the Hokusai Big Waterfall supercomputer facility and animal research facility of Rajiv Gandhi Centre for Biotechnology, Thiruvananthapuram for providing animals for conducting experiments. S.A. is thankful to VFSTR for analytical facilities at CoExAMMPC throughout the research work.

Appendix A. Supplementary data

Supplementary data to this article can be found online at https://doi.org/10.1016/j.csbj.2021.07.041.

References

[1] Walsh DM, Selkoe DJ. Deciphering the molecular basis of memory failure in Alzheimer's disease. Neuron 2004;44(1):181–93. https://doi.org/10.1016/j.neuron.2004.09.010.
[2] Scarpini E, Scheltens P, Feldman H. Treatment of alzheimer's disease: current status and new perspectives. Lancet Neurol 2003;2(9):539–47. https://doi.org/10.1016/s1474-4422(03)00502-7.
[3] Nunomura A, Castellani RJ, Zhu X, Moreira PI, Perry G, Smith MA. Involvement of oxidative stress in alzheimer disease. J Neuropathol Exp Neurol 2006;65(7):631–41. https://doi.org/10.1097/01.jnen.0000228136.58062.bf.
[4] Scheltens P, De Strooper B, Kivipelto M, Holstege H, Chételat G, Teunissen CE, et al. Alzheimer's disease. Lancet 2021;397(10284):1577–90. https://doi.org/10.1016/S0140-6736(20)32205-4.

[5] Davies P, Maloney AJ. Selective loss of central cholinergic neurons in Alzheimer's disease. Lancet 1976;2(8000):1403. https://doi.org/10.1016/s0140-6736(76)91936-x.
[6] Perry EK, Tomlinson BE, Blessed G, Bergmann K, Gibson PH, Perry RH. Correlation of cholinergic abnormalities with senile plaques and mental test scores in senile dementia. Br Med J 1978;2(6150):1457–9. https://doi.org/10.1136/bmj.2.6150.1457.
[7] Perry RH, Perry EK, Smith CJ, Xuereb JH, Irving D, Whitford CA, et al. Cortical neuropathological and neurochemical substrates of alzheimer's and parkinson's diseases. J Neural Transm Suppl 1987;24:131–6.
[8] Greenblatt HM, Dvir H, Silman I, Sussman JL. Acetylcholinesterase: a multifaceted target for structure-based drug design of anticholinesterase agents for the treatment of Alzheimer's disease. J Mol Neurosci 2003;20(3):369–83. https://doi.org/10.1385/JMN:20:3:369.
[9] Kryger G, Silman I, Sussman JL. Structure of acetylcholinesterase complexed with E2020 (Aricept): implications for the design of new anti-Alzheimer drugs. Structure 1999;7(3):297–307. https://doi.org/10.1016/s0969-2126(99)80040-9.
[10] Verma S, Kumar A, Tripathi T, Kumar A. Muscarinic and nicotinic acetylcholine receptor agonists: current scenario in Alzheimer's disease therapy. J Pharm Pharmacol 2018;70(8):985–93. https://doi.org/10.1111/jphp.12919.
[11] Koti Reddy E, Remya C, Sajith AM, Dileep KV, Sadasivan C, Anwar S. Functionaliseddihydroazo pyrimidine derivatives from Morita–Baylis–Hillman acetates: synthesis and studies against acetylcholinesterase as its inhibitors. RSC Adv 2016;6(81):77431–9. https://doi.org/10.1039/C6RA12507G.
[12] Sugimoto H. Donepezil hydrochloride: a treatment drug for Alzheimer's disease. Chem Rec 2001;1(1):63–73. https://doi.org/10.1002/(ISSN)1528-0691.
[13] Zarotsky V, Sramek JJ, Cutler NR. Galantamine hydrobromide: an agent for Alzheimer's disease. Am J Health Syst Pharm 2003;60(5):446–52. https://doi.org/10.1093/ajhp/60.5.446.
[14] Jann MW. Rivastigmine, a new-generation cholinesterase inhibitor for the treatment of Alzheimer's disease. Pharmacotherapy 2000;20(1):1–12. https://doi.org/10.1592/phco.20.1.1.34664.
[15] Wang R, Zhang HY, Tang XC. Huperzine A attenuates cognitive dysfunction and neuronal degeneration caused by beta-amyloid protein-(1–40) in rat. Eur J Pharmacol 2001;421(3):149–56. https://doi.org/10.1016/s0014-2999(01)01030-5.
[16] Law A, Gauthier S, Quirion R. Say NO to Alzheimer's disease: the putative links between nitric oxide and dementia of the Alzheimer's type. Brain Res Brain Res Rev 2001;35:73–96. https://doi.org/10.1016/S0165-0173(00)00051-5.
[17] Yankner BA, Lu T, Loerch P. The aging brain. Annu Rev Pathol 2008;3(1):41–66. https://doi.org/10.1146/annurev.pathmechdis.2.010506.092044.
[18] Choi DW. Excitotoxic cell death. J Neurobiol 1992;23(9):1261–76. https://doi.org/10.1002/(ISSN)1097-469510.1002/neu.v23:910.1002/neu.480230915.
[19] Lipton SA. NMDA receptors, glial cells, and clinical medicine. Neuron 2006;50(1):9–11. https://doi.org/10.1016/j.neuron.2006.03.026.
[20] Wang R, Reddy PH. Role of glutamate and NMDA receptors in Alzheimer's disease. J Alzheimers Dis 2017;57(4):1041–8. https://doi.org/10.3233/JAD-160763.
[21] Liu J, Chang L, Song Y, Li H, Wu Y. The role of NMDA receptors in Alzheimer's disease. Front Neurosci 2019;13:43. https://doi.org/10.3389/fnins.2019.00043.
[22] Olivares D, Deshpande VK, Shi Y, Lahiri DK, Greig NH, Rogers JT, et al. N-methyl D-aspartate (NMDA) receptor antagonists and memantine treatment for Alzheimer's disease, vascular dementia and Parkinson's disease. Curr Alzheimer Res 2012;9(6):746–58. https://doi.org/10.2174/156720512801322564.
[23] Amadoro G, Ciotti MT, Costanzi M, Cestari V, Calissano P, Canu N. NMDA receptor mediates tau-induced neurotoxicity by calpain and ERK/MAPK activation. Proc Natl Acad Sci USA 2006;103(8):2892–7. https://doi.org/10.1073/pnas.0511065103.
[24] Miguel-Hidalgo JJ, Alvarez XA, Cacabelos R, Quack G. Neuroprotection by memantine against neurodegeneration induced by beta-amyloid(1–40). Brain Res 2002;958(1):210–21. https://doi.org/10.1016/s0006-8993(02)03731-9.
[25] Talantova M, Sanz-Blasco S, Zhang X, Xia P, Akhtar MW, Okamoto S, et al. Abeta induces astrocytic glutamate release, extrasynaptic NMDA receptor activation, and synaptic loss. Proc Natl Acad Sci USA 2013;110(27):E2518–27. https://doi.org/10.1073/pnas.1306832110.
[26] Rogawski MA, Wenk GL. The neuropharmacological basis for the use of memantine in the treatment of Alzheimer's disease. CNS Drug Rev 2003;9:275–308. https://doi.org/10.1111/j.1527-3458.2003.tb00254.x.
[27] Molinuevo JL. Memantine: the value of combined therapy. Rev Neurol 2011;52(2):95–100.
[28] Molino, I., Colucci, L., Fasanaro, A.M., Traini, E. and Amenta, F., 2013. Efficacy of memantine, donepezil, or their association in moderate-severe Alzheimer's disease: a review of clinical trials. The Scientific World Journal, 2013.
[29] Guo J, Wang Z, Liu R, Huang Y, Zhang N, Zhang R. Memantine, donepezil, or combination therapy—What is the best therapy for Alzheimer's disease? A network meta-analysis. Brain Behav 2020;10(11). https://doi.org/10.1002/brb3.v10.1110.1002/brb3.1831.
[30] Kabir MT, Uddin MS, Mamun AA, Jeandet P, Aleya L, Mansouri RA, et al. Combination drug therapy for the management of Alzheimer's disease. Int J Mol Sci 2020;21(9):3272. https://doi.org/10.3390/ijms21093272.
[31] Deardorff WJ, Grossberg GT. A fixed-dose combination of memantine extended-release and donepezil in the treatment of moderate-to-severe Alzheimer's disease. Drug Design Dev Ther 2016;10:3267. https://doi.org/10.2147/DDDT.S86463.
[32] Atri A, Hendrix SB, Pejović V, Hofbauer RK, Edwards J, Molinuevo JL, et al. Cumulative, additive benefits of memantine-donepezil combination over component monotherapies in moderate to severe Alzheimer's dementia: a pooled area under the curve analysis. Alzheimer's Res Ther 2015;7(1):1–12. https://doi.org/10.1186/s13195-015-0109-2.
[33] Farinelli M, Heitz FD, Grewe BF, Tyagarajan SK, Helmchen F, Mansuy IM, et al. Selective regulation of NR2B by protein phosphatase-1 for the control of the NMDA receptor in neuroprotection. PLoS ONE 2012;7(3):e34047. https://doi.org/10.1371/journal.pone.0034047.
[34] Liu S-b, Zhang N, Guo Y-y, Zhao R, Shi T-y, Feng S-f, et al. G-protein-coupled receptor 30 mediates rapid neuroprotective effects of estrogen via depression of NR2B-containing NMDA receptors. J Neurosci 2012;32(14):4887–900. https://doi.org/10.1523/JNEUROSCI.5828-11.2012.
[35] Xie W, Stribley JA, Chatonnet A, Wilder PJ, Rizzino A, McComb RD, et al. Postnatal developmental delay and supersensitivity to organophosphate in gene-targeted mice lacking acetylcholinesterase. J Pharmacol Exp Ther 2000;293(3):896–902.
[36] Tu W, Xu X, Peng L, Zhong X, Zhang W, Soundarapandian MM, et al. DAPK1 interaction with NMDA receptor NR2B subunits mediates brain damage in stroke. Cell 2010;140(2):222–34. https://doi.org/10.1016/j.cell.2009.12.055.
[37] Park E, Bell JD, Baker AJ. Traumatic brain injury: can the consequences be stopped? CMAJ 2008;178(9):1163–70. https://doi.org/10.1503/cmaj.080282.
[38] Gao X, Wang H, Cai S, Saadatzadeh MR, Hanenberg H, Pollok KE, et al. Phosphorylation of NMDA 2B at S1303 in human glioma peritumoral tissue: implications for glioma epileptogenesis. Neurosurg Focus 2014;37(6):E17. https://doi.org/10.3171/2014.9.FOCUS14485.
[39] Lakhan SE, Caro M. Hadzimichalis N (2013) NMDA receptor activity in neuropsychiatric disorders. Front Psychiatry 2013;10(4):52. https://doi.org/10.3389/fpsyt.2013.00052.eCollection.
[40] Kannan G, Gressitt KL, Yang S, Stallings CR, Katsafanas E, Schweinfurth LA, Savage CLG, Adamos MB, Sweeney KM, Origoni AE, Khushalani S, Bahn S, Leweke FM, Dickerson FB, Yolken RH, Pletnikov MV, Severance EG (2017) Pathogen-mediated NMDA receptor autoimmunity and cellular barrier dysfunction in schizophrenia. Transl Psychiatry 7 (8):e1186. 10.1038/tp.2017.162
[41] Wu LJ, Zhuo M. Targeting the NMDA receptor subunit NR2B for the treatment of neuropathic pain. Neurotherapeutics 2009;6(4):693–702. https://doi.org/10.1016/j.nurt.2009.07.008.
[42] Kurz A. The therapeutic potential of tacrine. J Neural Transm Suppl 1998;54:295–9. https://doi.org/10.1007/978-3-7091-7508-8_29.
[43] Gracon SI, Knapp MJ, Berghoff WG, Pierce M, DeJong R, Lobbestael SJ, et al. Safety of tacrine: clinical trials, treatment IND, and postmarketing experience. Alzheimer Dis Assoc Disord 1998;12(2):93–101. https://doi.org/10.1097/00002093-199806000-00007.
[44] Hershkowitz N, Rogawski MA. Tetrahydroaminoacridine block of N-methyl-D-aspartate-activated cation channels in cultured hippocampal neurons. Mol Pharmacol 1991;39(5):592–8.
[45] Pang Y-P, Quiram P, Jelacic T, Hong F, Brimijoin S. Highly potent, selective, and low cost bis-tetrahydroaminacrine inhibitors of acetylcholinesterase. Steps toward novel drugs for treating Alzheimer's disease. J Biol Chem 1996;271(39):23646–9. https://doi.org/10.1074/jbc.271.39.23646.
[46] Rosini M, Andrisano V, Bartolini M, Bolognesi ML, Hrelia P, Minarini A, et al. Rational approach to discover multipotent anti-Alzheimer drugs. J Med Chem 2005;48(2):360–3. https://doi.org/10.1021/jm049112h10.1021/jm049112h.s001.
[47] Fang L, Appenroth D, Decker M, Kiehntopf M, Roegler C, Deufel T, et al. Synthesis and biological evaluation of NO-donor-tacrine hybrids as hepatoprotective anti-Alzheimer drug candidates. J Med Chem 2008;51(4):713–6. https://doi.org/10.1021/jm701491k.
[48] Fernández-Bachiller MI, Pérez C, Campillo NE, Páez JA, González-Muñoz GC, Usán P, et al. Tacrine-melatonin hybrids as multifunctional agents for Alzheimer's disease, with cholinergic, antioxidant, and neuroprotective properties. ChemMedChem 2009;4(5):828–41. https://doi.org/10.1002/cmdc.v4:510.1002/cmdc.200800414.
[49] Fernández-Bachiller MI, Pérez C, González-Muñoz GC, Conde S, López MG, Villarroya M, et al. Novel tacrine-8-hydroxyquinoline hybrids as multifunctional agents for the treatment of Alzheimer's disease, with neuroprotective, cholinergic, antioxidant, and copper-complexing properties. J Med Chem 2010;53(13):4927–37. https://doi.org/10.1021/jm100329q.
[50] Fernández-Bachiller MI, Pérez C, Monjas L, Rademann J, Rodríguez-Franco MI. New tacrine-4-oxo-4H-chromene hybrids as multifunctional agents for the treatment of Alzheimer's disease, with cholinergic, antioxidant, and β-amyloid-reducing properties. J Med Chem 2012;55(3):1303–17. https://doi.org/10.1021/jm201460y.
[51] Minarini A, Milelli A, Tumiatti V, Rosini M, Simoni E, Bolognesi ML, et al. Cystamine-tacrine dimer: a new multi-target-directed ligand as potential therapeutic agent for Alzheimer's disease treatment. Neuropharmacology 2012;62(2):997–1003. https://doi.org/10.1016/j.neuropharm.2011.10.007.
[52] Thiratmatrakul S, Yenjai C, Waiwut P, Vajragupta O, Reubroycharoen P, Tohda M, et al. Synthesis, biological evaluation and molecular modeling study of novel tacrine-carbazole hybrids as potential multifunctional agents for the

treatment of Alzheimer's disease. Eur J Med Chem 2014;75:21–30. https://doi.org/10.1016/j.ejmech.2014.01.020.
[53] Nepovimova E, Korabecny J, Dolezal R, Babkova K, Ondrejicek A, Jun D, et al. Tacrine-trolox hybrids: a novel class of centrally active, nonhepatotoxic multi-target-directed ligands exerting anticholinesterase and antioxidant activities with low in vivo toxicity. J Med Chem 2015;58(22):8985–9003. https://doi.org/10.1021/acs.jmedchem.5b01325.
[54] Zhang C, Du Q-Y, Chen L-D, Wu W-H, Liao S-Y, Yu L-H, et al. Design, synthesis and evaluation of novel tacrine-multialkoxybenzene hybrids as multi-targeted compounds against Alzheimer's disease. Eur J Med Chem 2016;116:200–9. https://doi.org/10.1016/j.ejmech.2016.03.077.
[55] Reddy EK, Remya C, Mantosh K, Sajith AM, Omkumar RV, Sadasivan C, et al. Novel tacrine derivatives exhibiting improved acetylcholinesterase inhibition: Design, synthesis and biological evaluation. Eur J Med Chem 2017;139:367–77. https://doi.org/10.1016/j.ejmech.2017.08.013.
[56] Zhou J, Jiang X, He S, Jiang H, Feng F, Liu W, et al. Rational design of multitarget-directed ligands: strategies and emerging paradigms. J Med Chem 2019;62(20):8881–914. https://doi.org/10.1021/acs.jmedchem.9b00017.
[57] Agis-Torres A, Solhuber M, Fernandez M, Sanchez-Montero JM. Multi-target-directed ligands and other therapeutic strategies in the search of a real solution for Alzheimer's disease. Curr Neuropharmacol 2014;12(1):2–36. https://doi.org/10.2174/1570159X113116660047.
[58] Bajda M, Guzior N, Ignasik M, Malawska B. Multi-target-directed ligands in Alzheimer's disease treatment. Curr Med Chem 2011;18(32):4949–75. https://doi.org/10.2174/092986711797535245.
[59] Guzior N, Wieckowska A, Panek D, Malawska B. Recent development of multifunctional agents as potential drug candidates for the treatment of Alzheimer's disease. Curr Med Chem 2015;22(3):373–404. https://doi.org/10.2174/0929867321666141106122628.
[60] Schneider LS, Geffen Y, Rabinowitz J, Thomas RG, Schmidt R, Ropele S, et al. Low-dose ladostigil for mild cognitive impairment: a phase 2 placebo-controlled clinical trial. Neurology 2019;93(15):e1474–84. https://doi.org/10.1212/WNL.0000000000008239.
[61] Perez DI, Martinez A, Gil C, Campillo EN. From bitopic inhibitors to multitarget drugs for the future treatment of Alzheimer's disease. Curr Med Chem 2015;22(33):3789–806. https://doi.org/10.2174/0929867322666150812145825.
[62] Benek O, Korabecny J, Soukup O. A perspective on multi-target drugs for Alzheimer's disease. Trends Pharmacol Sci 2020;41(7):434–45. https://doi.org/10.1016/j.tips.2020.04.008.
[63] Gorecki L, Misiachna A, Damborsky J, Dolezal R, Korabecny J, Cejkova L, et al. Structure-activity relationships of dually-acting acetylcholinesterase inhibitors derived from tacrine on N-methyl-d-Aspartate receptors. Eur J Med Chem 2021;219:113434. https://doi.org/10.1016/j.ejmech.2021.113434.
[64] Konecny J, Misiachna A, Hrabinova M, Pulkrabkova L, Benkova M, Prchal L, et al. Pursuing the complexity of Alzheimer's disease: discovery of fluoren-9-amines as selective butyrylcholinesterase inhibitors and n-methyl-d-aspartate receptor antagonists. Biomolecules 2021;11(1):3. https://doi.org/10.3390/biom11010003.
[65] Kaniakova M, Kleteckova L, Lichnerova K, Holubova K, Skrenkova K, Korinek M, et al. 7-Methoxyderivative of tacrine is a 'foot-in-the-door'open-channel blocker of GluN1/GluN2 and GluN1/GluN3 NMDA receptors with neuroprotective activity in vivo. Neuropharmacology 2018;140:217–32. https://doi.org/10.1016/j.neuropharm.2018.08.010.
[66] Kaniakova M, Korabecny J, Holubova K, Kleteckova L, Chvojkova M, Hakenova K, et al. 7-phenoxytacrine is a dually acting drug with neuroprotective efficacy in vivo. Biochem Pharmacol 2021;186:114460. https://doi.org/10.1016/j.bcp.2021.114460.
[67] Karakas E, Simorowski N, Furukawa H. Subunit arrangement and phenylethanolamine binding in GluN1/GluN2B NMDA receptors. Nature 2011;475(7355):249–53. https://doi.org/10.1038/nature10180.
[68] Regan MC, Zhu Z, Yuan H, Myers SJ, Menaldino DS, Tahirovic YA, et al. Structural elements of a pH-sensitive inhibitor binding site in NMDA receptors. Nat Commun 2019;10(1). https://doi.org/10.1038/s41467-019-08291-1.
[69] Zhu S, Stein RA, Yoshioka C, Lee CH, Goehring A, Mchaourab HS, et al. Mechanism of NMDA receptor inhibition and activation. Cell 2016;165(3):704–14. https://doi.org/10.1016/j.cell.2016.03.028.
[70] Lee CH, Lü W, Michel JC, Goehring A, Du J, Song X, et al. NMDA receptor structures reveal subunit arrangement and pore architecture. Nature 2014;511(7508):191–7. https://doi.org/10.1038/nature13548.
[71] Albin RL, Young AB, Penney JB. Tetrahydro-9-aminoacridine (THA) interacts with the phencyclidine (PCP) receptor site. Neurosci Lett 1988;88(3):303–7. https://doi.org/10.1016/0304-3940(88)90228-5.
[72] Mayer ML. Crystal structures of the GluR5 and GluR6 ligand binding cores: molecular mechanisms underlying kainate receptor selectivity. Neuron 2005;45(4):539–52. https://doi.org/10.1016/j.neuron.2005.01.031.
[73] Nowak L, Bregestovski P, Ascher P, Herbet A, Prochiantz A. Magnesium gates glutamate-activated channels in mouse central neurones. Nature 1984;307(5950):462–5. https://doi.org/10.1038/307462a0.
[74] Honey CR, Miljkovic Z, MacDonald JF. Ketamine and phencyclidine cause a voltage-dependent block of responses to L-aspartic acid. Neurosci Lett 1985;61(1–2):135–9. https://doi.org/10.1016/0304-3940(85)90414-8.
[75] Huettner JE, Bean BP. Block of N-methyl-D-aspartate-activated current by the anticonvulsant MK-801: selective binding to open channels. Proc Natl Acad Sci USA 1988;85(4):1307–11. https://doi.org/10.1073/pnas.85.4.1307.
[76] MacDonald JF, Bartlett MC, Mody I, Pahapill P, Reynolds JN, Salter MW, Schneiderman JH, Pennefather PS (1991) Actions of ketamine, phencyclidine and MK-801 on NMDA receptor currents in cultured mouse hippocampal neurones. J Physiol 432:483-508. 10.1113/jphysiol.1991.sp018396
[77] Zheng W, Wen H, Iacobucci GJ, Popescu GK. Probing the structural dynamics of the NMDA receptor activation by coarse-grained modeling. Biophys J 2017;112(12):2589–601. https://doi.org/10.1016/j.bpj.2017.04.043.
[78] Cheung J, Rudolph MJ, Burshteyn F, Cassidy MS, Gary EN, Love J, et al. Structures of human acetylcholinesterase in complex with pharmacologically important ligands. J Med Chem 2012;55(22):10282–6. https://doi.org/10.1021/jm300871x.
[79] Clark DE. Rapid calculation of polar molecular surface area and its application to the prediction of transport phenomena. 2. Prediction of blood-brain barrier penetration. J Pharm Sci 1999;88(8):815–21. https://doi.org/10.1021/js980402t.
[80] Remya C, Dileep KV, Tintu I, Variyar EJ, Sadasivan C. In vitro inhibitory profile of NDGA against AChE and its in silico structural modifications based on ADME profile. J Mol Model 2013;19(3):1179–94. https://doi.org/10.1007/s00894-012-1656-0.
[81] Hu MK, Wu LJ, Hsiao G, Yen MH. Homodimeric tacrine congeners as acetylcholinesterase inhibitors. J Med Chem 2002;45(11):2277–82. https://doi.org/10.1021/jm010308g.
[82] Chandrika AR, Steephan M, Raveendran Nair R, Sudarsana Devi SP, Kumar M, Paul S, et al. A simple end-point assay for calcium channel activity. Cell Calcium 2018;74:73–85. https://doi.org/10.1016/j.ceca.2018.05.009.
[83] Sassa S, Sugita O, Galbraith RA, Kappas A. Drug metabolism by the human hepatoma cell, Hep G2. BiochemBiophys Res Commun 1987;143(1):52–7. https://doi.org/10.1016/0006-291x(87)90628-0.
[84] Ramirez T, Strigun A, Verlohner A, Huener H-A, Peter E, Herold M, et al. Prediction of liver toxicity and mode of action using metabolomics in vitro in HepG2 cells. Arch Toxicol 2018;92(2):893–906. https://doi.org/10.1007/s00204-017-2079-6.
[85] Thabrew MI, Hughes RD, McFarlane IG. Screening of hepatoprotective plant components using a HepG2 cell cytotoxicity assay. J Pharm Pharmacol 1997;49(11):1132–5. https://doi.org/10.1111/j.2042-7158.1997.tb06055.x.
[86] Brewer GJ, Torricelli JR, Evege EK, Price PJ. Optimized survival of hippocampal neurons in B27-supplemented Neurobasal, a new serum-free medium combination. J Neurosci Res 1993;35(5):567–76. https://doi.org/10.1002/jnr.490350513.
[87] Campos-Esparza MR, Sanchez-Gomez MV, Matute C. Molecular mechanisms of neuroprotection by two natural antioxidant polyphenols. Cell Calcium 2009;45(4):358–68. https://doi.org/10.1016/j.ceca.2008.12.007.
[88] Lesuisse C, Martin LJ. Immature and mature cortical neurons engage different apoptotic mechanisms involving caspase-3 and the mitogen-activated protein kinase pathway. J Cereb Blood Flow Metab 2002;22(8):935–50. https://doi.org/10.1097/00004647-200208000-00005.
[89] Kim HN, Jang JY, Choi BT. A single fraction from Uncariasinensis exerts neuroprotective effects against glutamate-induced neurotoxicity in primary cultured cortical neurons. Anat Cell Biol 2015;48(2):95–103. https://doi.org/10.5115/acb.2015.48.2.95.
[90] Remya C, Dileep KV, Variyar EJ, Zhang KYJ, Omkumar RV, Sadasivan C. Chemical similarity assisted search for acetylcholinesterase inhibitors: molecular modeling and evaluation of their neuroprotective properties. Int J Biol Macromol 2021;174:466–76. https://doi.org/10.1016/j.ijbiomac.2021.01.148.
[91] Matus A, Bernhardt R, Bodmer R, Alaimo D. Microtubule-associated protein 2 and tubulin are differently distributed in the dendrites of developing neurons. Neuroscience 1986;17(2):371–89. https://doi.org/10.1016/0306-4522(86)90253-8.
[92] Nakao N, Nokaia Z, Odin P, Lindvall O. Protective effects of BDNF and NT-3 but not PDGF against hypoglycemic injury to cultured striatal neurons. Exp Neurol 1995;131(1):1–10. https://doi.org/10.1016/0014-4886(95)90002-0.
[93] Ryu JK, Cho T, Wang Y, McLarnon JG. Neural progenitor cells attenuate inflammatory reactivity and neuronal loss in an animal model of inflamed AD brain. J Neuroinflamm 2009;6(1):39. https://doi.org/10.1186/1742-2094-6-39.
[94] Park CH, Choi SH, Piao Y, Kim S-H, Lee Y-J, Kim H-S, et al. Glutamate and aspartate impair memory retention and damage hypothalamic neurons in adult mice. Toxicol Lett 2000;115(2):117–25. https://doi.org/10.1016/S0378-4274(00)00188-0.
[95] Olney JW. Brain lesions, obesity, and other disturbances in mice treated with monosodium glutamate. Science 1969;164(3880):719–21. https://doi.org/10.1126/science.164.3880.719.
[96] Gonzalez-Burgos I, Velazquez-Zamora DA, Beas-Zarate C. Damage and plasticity in adult rat hippocampal trisynaptic circuit neurons after neonatal exposure to glutamate excitotoxicity. Int J Dev Neurosci 2009;27(8):741–5. https://doi.org/10.1016/j.ijdevneu.2009.08.016.
[97] Ma J, Yu LJ, Ma RD, Zhang YP, Fang JZ, Zhang XY, et al. Repair of glutamate-induced excitotoxic neuronal damage mediated by intracerebroventricular transplantation of neural stem cells in adult mice. Neurosci Bull 2007;23(4):209–14. https://doi.org/10.1007/s12264-007-0031-0.

[98] James O, Yetunde A. Acute low dose monosodium glutamate retards novelty induced behaviours in male Swiss albino mice. J Neurosci Behav Health 2011;3(4):51–6. https://doi.org/10.5897/JNBH.9000001.
[99] Wagstaff AJ, McTavish D (1994) Tacrine. A review of its pharmacodynamic and pharmacokinetic properties, and therapeutic efficacy in Alzheimer's disease. Drugs Aging 4 (6):510-540. 10.2165/00002512-199404060-00006
[100] Ma C, Wang L, Yang P, Myint KZ, Xie XQ. LiCABEDS II. Modeling of ligand selectivity for G-protein-coupled cannabinoid receptors. J Chem Inf Model 2013;53(1):11–26. https://doi.org/10.1021/ci3003914.
[101] Viayna E, Coquelle N, Cieslikiewicz-Bouet M, Cisternas P, Oliva CA, Sánchez-López E, et al. Discovery of a potent dual inhibitor of acetylcholinesterase and butyrylcholinesterase with antioxidant activity that alleviates Alzheimer-like pathology in old APP/PS1 mice. J Med Chem 2021;64(1):812–39. https://doi.org/10.1021/acs.jmedchem.0c01775.
[102] Greig NH, Utsuki T, Ingram DK, Wang Y, Pepeu G, Scali C, et al. Selective butyrylcholinesterase inhibition elevates brain acetylcholine, augments learning and lowers Alzheimer β-amyloid peptide in rodent. Proc Natl Acad Sci 2005;102(47):17213–8. https://doi.org/10.1073/pnas.0508575102.
[103] Košak U, Brus B, Knez D, Šink R, Žakelj S, Trontelj J, et al. Development of an in-vivo active reversible butyrylcholinesterase inhibitor. Sci Rep 2016;6(1). https://doi.org/10.1038/srep39495.
[104] Darvesh S, Hopkins DA, Geula C. Neurobiology of butyrylcholinesterase. Nat Rev Neurosci 2003;4(2):131–8. https://doi.org/10.1038/nrn1035.
[105] Kumar A, Pintus F, Di Petrillo A, Medda R, Caria P, Matos MJoão, et al. Novel 2-pheynlbenzofuran derivatives as selective butyrylcholinesterase inhibitors for Alzheimer's disease. Sci Rep 2018;8(1). https://doi.org/10.1038/s41598-018-22747-2.
[106] Arias E, Ales E, Gabilan NH, Cano-Abad MF, Villarroya M, Garcia AG, et al. Galantamine prevents apoptosis induced by beta-amyloid and thapsigargin: involvement of nicotinic acetylcholine receptors. Neuropharmacology 2004;46(1):103–14. https://doi.org/10.1016/s0028-3908(03)00317-4.
[107] Cocconcelli G, Diodato E, Caricasole A, Gaviraghi G, Genesio E, Ghiron C, et al. Aryl azoles with neuroprotective activity–parallel synthesis and attempts at target identification. Bioorg Med Chem 2008;16(4):2043–52. https://doi.org/10.1016/j.bmc.2007.10.090.
[108] Song X, Jensen MO, Jogini V, Stein RA, Lee CH, McHaourab HS, et al. Mechanism of NMDA receptor channel block by MK-801 and memantine. Nature 2018;556(7702):515–9. https://doi.org/10.1038/s41586-018-0039-9.
[109] Suhre K, Sanejouand YH (2004) ElNemo: a normal mode web server for protein movement analysis and the generation of templates for molecular replacement. Nucleic Acids Res 32 (Web Server issue):W610-614. 10.1093/nar/gkh368
[110] Grant BJ, Rodrigues AP, ElSawy KM, McCammon JA, Caves LS. Bio3d: an R package for the comparative analysis of protein structures. Bioinformatics 2006;22(21):2695–6. https://doi.org/10.1093/bioinformatics/btl461.
[111] Lopez-Blanco JR, Garzon JI, Chacon P. iMod: multipurpose normal mode analysis in internal coordinates. Bioinformatics 2011;27(20):2843–50. https://doi.org/10.1093/bioinformatics/btr497.
[112] McCoy AJ, Nicholls RA, Schneider TR. SCEDS: protein fragments for molecular replacement in Phaser. Acta Crystallogr D Biol Crystallogr 2013;69 (11):2216–25. https://doi.org/10.1107/S0907444913021811.
[113] Tiwari SP, Fuglebakk E, Hollup SM, Skjærven L, Cragnolini T, Grindhaug SH, et al. WEBnm@ v2.0: Web server and services for comparing protein flexibility. BMC Bioinf 2014;15:427. https://doi.org/10.1186/s12859-014-0427-6.
[114] Li Y, Zhang Y. REMO: A new protocol to refine full atomic protein models from C-alpha traces by optimizing hydrogen-bonding networks. Proteins 2009;76(3):665–76. https://doi.org/10.1002/prot.22380.
[115] Harder E, Damm W, Maple J, Wu C, Reboul M, Xiang JY, et al. OPLS3: a force field providing broad coverage of drug-like small molecules and proteins. J Chem Theory Comput 2016;12(1):281–96. https://doi.org/10.1021/acs.jctc.5b00864.
[116] Gerlits O, Ho K-Y, Cheng X, Blumenthal D, Taylor P, Kovalevsky A, et al. A new crystal form of human acetylcholinesterase for exploratory room-temperature crystallography studies. Chem Biol Interact 2019;309:108698. https://doi.org/10.1016/j.cbi.2019.06.011.
[117] Daina A, Michielin O, Zoete V. SwissADME: a free web tool to evaluate pharmacokinetics, drug-likeness and medicinal chemistry friendliness of small molecules. Sci Rep 2017;7:42717. https://doi.org/10.1038/srep42717.
[118] Liu H, Wang L, Lv M, Pei R, Li P, Pei Z, et al. AlzPlatform: an Alzheimer's disease domain-specific chemogenomics knowledgebase for polypharmacology and target identification research. J Chem Inf Model 2014;54(4):1050–60. https://doi.org/10.1021/ci500004h.
[119] Sussman JL, Harel M, Frolow F, Oefner C, Goldman A, Toker L, et al. Atomic structure of acetylcholinesterase from Torpedo californica: a prototypic acetylcholine-binding protein. Science 1991;253(5022):872–9. https://doi.org/10.1126/science.1678899.
[120] Bon S, Vigny M, Massoulie J. Asymmetric and globular forms of acetylcholinesterase in mammals and birds. Proc Natl Acad Sci USA 1979;76(6):2546–50. https://doi.org/10.1073/pnas.76.6.2546.
[121] Ellman GL, Courtney KD, Andres V, Featherstone RM. A new and rapid colorimetric determination of acetylcholinesterase activity. BiochemPharmacol 1961;7(2):88–95. https://doi.org/10.1016/0006-2952(61)90145-9.
[122] Morris R. Developments of a water-maze procedure for studying spatial learning in the rat. J Neurosci Methods 1984;11(1):47–60. https://doi.org/10.1016/0165-0270(84)90007-4.